SEISMIC NEAR FIELD OF AN AIR GUN MEASURED BY A WIDE BAND ACCELEROMETER SYSTEM

by
Paul Allen Reasenberg
B.A., Cornell University
(1967)

SUBMITTED IN
PARTIAL FULFILLMENT
OF THE REQUIREMENTS FOR THE
DEGREE OF MASTER OF SCIENCE
at the
MASSACHUSETTS INSTITUTE OF
TECHNOLOGY
September, 1971

Signature of Author.....
Department of Earth and Planetary Sciences
August 16, 1971

Certified by.....
Thesis Supervisor

Accepted by.....
Chairman, Departmental Committee
on Graduate Students

SEISMIC NEAR FIELD OF AN AIR GUN MEASURED BY A WIDE BAND ACCELEROMETER SYSTEM

by
Paul Allen Reasenberg

Submitted to the Department of Earth and Planetary Sciences on August 16, 1971 in partial fulfillment of the requirement for the degree of Master of Science

ABSTRACT

A portable accelerometer system was developed to detect, telemeter and record the ground accelerations at three points around a seismic event. The system consists of two remote sensing stations and a local sensing and recording station. At each station, 3 components of acceleration are processed by active filters to give band limited acceleration (.1 to 25 Hz.) and displacement (.01 to 10 Hz) signals. Telemetering to the local station is by FM radio link. To test the telemetering system in the field, an experiment was performed in which an air gun was periodically fired in a water filled hole in a granite quarry in Chelmsford, Massachusetts. The accelerometer system monitored the seismic near field (8 to 21 m) of the air gun. The averaged recorded amplitudes agree within less than an order of magnitude with a theoretical estimate using Sharpe's (1942) model of an explosive source. A similar analysis by Heelan (1953) which neglects the near field terms is inadequate at these close distances. SH motions were also generated. Possible source mechanisms of these motions include the eccentric placement of the gun in the hole, and the assymetric release of air by the gun. The telemetry system performance was basically satisfactory. S/N ratio in the acceleration channels was 54 db. Interchannel separation was greater than 60 db.

Thesis Supervisor: Keiiti Aki
Title: Professor of Geophysics

TABLE OF CONTENTS

	PAGE
ABSTRACT	
INTRODUCTION	4
INSTRUMENTATION	4
EXPERIMENT	22
CONCLUSIONS	31
ACKNOWLEDGEMENTS	33
REFERENCES	34
TABLES	35
FIGURE CAPTIONS	43
FIGURES	45

INTRODUCTION

A wide band accelerometer system was developed to detect, telemeter and record the ground motion at three points surrounding a seismic event. In order to test the system for field application, we recorded the seismic near field of an air gun which was operated in a water filled hole in a Massachusetts granite quarry. This thesis describes the accelerometer system, its function and the result obtained by the system during the air gun experiment.

INSTRUMENTATION

A. General Description

The purpose of the M. I. T. Seismic Telemetry System is to provide wide-band azimuthal coverage in the near field of a seismic event. Simultaneous detection and recording of ground motion at three points is now possible, and a fourth station will be added during the next year. The system (Figures 1 through 8) is composed of three stations. Each of two Remote Data Stations detect three orthogonal components of ground motion, perform signal processing on them and telemeter the data by FM radio to a Local Data Station. The Local Data Station detects three components of ground motion as well, and similarly performs signal processing. However, instead of transmitting its data, the Local Data Station receives the radio signals from the two Remote Data Stations, and acts as a meeting place for the three sets of data.

In each data station, the ground motion sensors are force balanced accelerometers. The signals from these three orthogonal sensors are directly proportional to ground acceleration. Two types of signal processing are done in each data station. One active filter for each component performs a double integration and amplifies the signal to give an output proportional to ground displacement. The other active filter is a band pass filter, whose output is proportional to ground acceleration. Hence, six data signals originate from each data station. Each of the six data signals drives a Voltage Controlled Oscillator (VCO) to produce six frequency modulated data subcarriers.. In the Remote Data Stations, the combined subcarriers (called the multiplex signal) modulate an FM transmitter which transmits through a directional antenna. In the Local Data Station the data remains in multiplex form.

From the Local Data Station, the three multiplex signals (one locally generated, two received by radio) pass to the Recording and Discriminating Unit (RDU). Here, each multiplex signal is mixed with a crystal controlled reference frequency for tape speed compensation and sent to the Tape Unit to be recorded.

During playback of the tape, one multiplex signal at a time is discriminated, with the use of a reference discriminator and six data discriminators. The data discriminator outputs return the six original data signals.

A 1/2-second time mark generator in the Local Data Station provides a timing signal which is recorded on one track of the Tape Unit. A WWV radio receiver signal is recorded on another tape trace for precise,absolute timing.

Power is supplied to each data station by a series combination of car batteries to give 30 V.D.C. Power for the Tape Unit and Recording and Discriminating Unit must be 110 V.A.C., either 50 or 60 cycles per second.

B. Mechanical Description

The data stations are housed in weather-tight aluminum cases, measuring 17" deep x 20 1/2" wide x 11 1/2" high, including connectors. The Remote Data Stations weigh 32 pounds each. The Local Data Station weighs 34 pounds.

The Recording and Discriminating Unit is housed in a deep aluminum case, measuring 15" x 9 1/2" x 25 1/2", and weighing 63 pounds.

The Tape Unit is an Ampex FR-1300. Its dimensions are 24" x 18" x 12 1/2". It weighs approximately 110 pounds.

C. System Description

1. Accelerometers

Each station has three Systron-Donner model 4310 accelerometers - two horizontal and one vertical. Each accelerometer's full scale range is $\pm$ 1g. and the nominal full scale output is $\pm$ 7.5 volts. Output impedance is about 5 k. $\pm$ 15 volt power is supplied to each accelerometer. Natural frequency is about 150 Hz. and damping, achieved electrically, is

.7 times critical. Frequency response is flat from D.C to over 100 Hz.

The three accelerometers are mounted mutually orthogonally on the base of a sealed aluminum container. On the flange at the base of the container are eight mounting bolt holes. These holes may also be used to align the accelerometers. Two holes have stamped marks next to them; one is stamped "L" and one "T". Horizontal accelerations in the directions from the center of the base to the centers of the "L" and "T" holes will produce positive output voltages in the Longitudinal and Transverse component accelerometers, respectively. An upward acceleration will produce a positive output voltage in the vertical component accelerometer.

2. Internal Calibrator

The internal calibration circuit consists of a fixed frequency (3 Hz.) oscillator and an operational amplifier follower. Output voltage is normally set to 15 volts peak to peak (corresponding to a $\pm$ 1g. sinusoidal input). A fine gain adjustment is located inside the station case. 24-V.D.C. power to the 3Hz. oscillator is controlled by a switch on the front panel. The calibrator signal may be applied to any combination of the three sets of filters by setting the appropriate input selector switches on the front panel to INT CAL.

In addition to the internal calibrator, an external calibration signal may be applied to the EXTERNAL CAL INPUT

jack on the front panel. Setting the filter input selector switches to EXT CAL then applies this signal to the filters.

Note that all the calibrations start at the filter inputs. No transducer calibration is provided.

3. A-Filter

This filter is intended for data in the frequency band .01 to 10 Hz. In this band, the frequency response is nearly equal to an ideal double integrator (slope of 12 db per octave). The response is shown in Figure 9. Low frequency high-pass sections remove the D.C. response, thereby eliminating the necessity of precise leveling of the sensors and removing drift. Maximum gain is 12,000 at .008 Hz. Unity gain is at about 2 Hz. The output of this filter is proportional to displacement within the range .01 to 10 Hz. The displacement at 0.1 Hz. corresponding to a full scale output ($\pm$ 2.5 volts) is $\pm$ 2.5 cm, when the Systron-Donner 4310 accelerometers are used. The electrical characteristics are summarized in Table 1.

4. B-Filter

The B filter is a band pass filter intended for data in the range .1 to 25 Hz. The response within the passband is (Fig. 10) essentially flat, with a gain of 1/3. The high cut slope is 18 db per octave, beginning at 25 Hz. The low cut slope, which is 6 db per octave beginning at .025 Hz. eliminates the need for precise accelerometer leveling and removes drift. The output voltage is proportional to accelera-

tion. Full scale ± 1 g. input acceleration produces full scale ± 2.5 volts at the output, when the Systron-Donner 4310 accelerometers are used. The electrical characteristics are summarized in Table 2.

5. Voltage Controlled Oscillators and Mixer Amplifiers

The output of each of the six filters drives the analog input of a voltage controlled oscillator (VCO). They are I.E.D. model CSO-300-1 oscillators. The VCO center frequencies are 2.3, 3.3, 4.3, 5.3, 6.3, and 7.3 kHz. Full frequency deviation for each VCO is ±250 Hz., which is produced by full scale inputs of ± 2.5 volts. The six output subcarriers are combined in an I.E.D. CMA-400 mixing amplifier and the complete multiplex signal is used to modulate the transmitter.

6. Transmitters and Receivers

Each of the two Remote Data Stations has a transmitter. They are Conic Corp. model CTM-405k 5 watt FM telemetry transmitters. Carrier frequencies are 377.5 MHz. and 391.5 MHz. Power is supplied from the regulated 25 volt supply and controlled by a switch on the front panel.

The Local Data Station contains two Conic Corp. model CAR-210 FM receivers, one tuned to each of the above frequencies. A meter on the front panel of the Local Data Station indicates the strength of the received r.f. signal in each of two receivers. Power to the receivers is controlled by a switch on the front panel. The radio link characteristics

are summarized in Tables 3 and 4.

7. Antennas

The transmitting antennas are specially designed and tuned. They are Decibel Products model DB-402. They both nominally cover the frequency range 377-391 MHz. Each consists of two stacked elements on a vertical mast. Radiation is vertically polarized, and the horizontal radiation pattern is elliptical. Forward gain is +6 db above a half-wave dipole. Impedance is 50 ohms.

The receiving antenna is Decibel Products model DB-404 SP. It is an omni-directional antenna for 377-391 MHz. consisting of two double elements stacked on a vertical mast. Two receivers are fed from this antenna by means of a T-connector in the transmission line. Impedance is 50 ohms.

8. Recording and Discriminating Unit (RDU)

a. Recording

The left most plug-in module in the RDU is the E.M.R. model 4810 Reference oscillator and Amplifier. The top of this module is a stable reference oscillator operating at 17 KHz. The bottom half is a two-input broad-band mixing amplifier. It consists of two identical amplifiers, each of which is identical to the 4810 amplifier section. These three amplifiers each amplify and mix one multiplex signal coming from the Local Data Station with the 17 KHz.reference tone. The three composite outputs are sent via coaxial cables to the record inputs of channels 1, 2 and 3 of the Ampex

FR-1300 tape recorder. The purpose of adding the 17 KHz. tone to the multiplex is to provide a reference frequency for tape speed error compensation after playback.

b. Discriminating

The third and fourth modular spaces from the left contain the E.M.R. model 4130/4131-51 reference discriminator. The reproduced multiplex signal from the tape recorder first passes through this unit, where the 17 KHz. signal is separated and demodulated. The demodulated signal equals zero except when speed fluctuations in the tape recorder frequency-modulate the reference tone. Thus, this signal is an analog representation of the tape speed error. This signal is called the tape speed compensation (TSC). Meanwhile, the multiplex data in the reference discriminator must undergo a time delay to assure that the TSC is applied at the proper time in the data discriminators. Upon leaving the reference discriminator, the delayed multiplex signal enters all six data discriminators.

The last six modular units are E.M.R. model 4150 data discriminators. Each one consists of a band-pass input filter (BPIF) tuned to a particular subcarrier band, an FM discriminator, and a low-pass output filter (LPOF) with a cutoff frequency of 25 Hz. The six BPIF's are each tuned to a different subcarrier band, and the FM discriminators have corresponding center frequencies (which are the same as the VCO center frequencies - 2.3, 3.3, 4.3, 5.3, 6.3 and 7.3 KHz.).

The TSC signal is also applied to each data discriminator, and tape speed error correction is made here. The LPOF's reduce any noise outside the data pass-band.

In the jack-panel above the modular units are coaxial output connectors. Jacks labeled TIME and WWV provide 1/2 second timing marks and the WWV receiver audio output as reproduced from the tape recorder. Jacks labeled LA, LB, TA, TB, VA, VB provide the data outputs from the six data discriminators below them (i.e., LA is the output of the 2.3 KHz. discriminator, and VB is the output of the 7.3 KHz. discriminator).

9. 1/2-Second Time Mark Generator

Inside the Local Data Station is an astable multivibrator, which produces a time mark pulse every half second. This signal goes directly onto one track of the Tape Unit.

10. WWV Receiver

A portable, battery operated radio receiver (Specific Products model WWVT) is used to provide accurate absolute timing signals from WWV. The audio output from the receiver is recorded directly on one track of the tape unit.

11. Tape Unit

The Tape Unit is an Ampex model FR-1300 7-track portable recorder. It records on 1/2-inch magnetic tape. Tape speeds are switchable, and a recording speed of 3 3/4 or 7 1/2 inches per second may be used in this system. Recording time at 3 3/4 i.p.s. with 3600 foot tapes is 3 hours.

Electronics for the multiplex data channels are direct record and reproduce, while electronics for all other channels are FM record and reproduce.

12. Power Supplies

In each data station, several regulated power supplies provide the voltages needed by the station's components. All the power supplies begin with the 30 V.D.C. from the car batteries.

A Technipower model CX-95 series regulator provides a nominal 24 volts for the transmitters, receivers, calibrator, and pump. The RA-TEK model P-1 pump runs off the 24 volt supply and provides the 455 kc. oscillator signal to run the parametric amplifiers in the A-filters. The P-1 pump also supplies a regulated nominal 19 volts to the parametric amps. A Transformer Electronics Co. model 9646-101 Dual Converter generates balanced $\pm$ 21 volts, which in turn supplies a Philbrick Dual Regulator, model 2101. This provides regulated $\pm$ 15 V.D.C. for the operational amplifiers in the filters, the operational amplifier in the calibrate circuit, and the accelerometers. All the power supply modules are mounted on a fiberglass sub-chassis in each data station.

D. Principles of Operation

1. Signal-to-noise Ratio

One of the major sources of noise is attributable to the tape recorder. The noise arises from two separate areas of the recorder and can be classified as "amplitude noise"

generated within the pass band of the direct — record electronics and as "frequency modulation noise" created by the wow and flutter characteristics of the machine. The noise components introduced by the radio link will be discussed in another section.

a. Amplitude Noise

The Ampex FR-1300 tape recorder provides a 30 db broadband signal-to-noise figure over a bandwidth of 38 kHz. at tape speed of 7.5 i.p.s. Assuming this noise is evenly distributed over the passband, the data discriminator output signal-to-noise ratio from this noise source can be computed following the analysis by EMR Telemetry, Inc. (1970):

S_i = the rms voltage of the FM subcarrier, and

N_i = the rms noise out of the discriminator input filter.

B_T = the tape recorder bandwith or 38 kHz.

B_C = the data channel bandwith or 500 Hz.

Then, $\frac{S_i}{N_i} = 30 \text{ db} + 20 \log_{10} \left(\frac{38 \times 10^3}{5 \times 10^2}\right)^{1/2} = 49 \text{ db}.$

$$\frac{S_o}{N_o} = \sqrt{3} \cdot \beta^{3/2} \frac{S_i}{N_i}$$

where S_o = the maximum rms sinewave output data signal,

N_o = the rms output noise due to pass band noise,

β = the deviation ratio, i.e., one half of the total

FM bandwidth divided by the maximum data frequency. S_i/N_i is the S/N ratio of the multiplex signal at the input to the discriminators. It does not take into account the number of subcarriers, n, which comprise it. For equal amplitude subcarriers, $\frac{S_i}{N_i}$ for each subcarrier is $\frac{1}{n}$ times that for the multiplex. In our system, there are 6 data subcarriers and one double amplitude reference subcarrier. Hence, n = 8 and

$$\frac{S_i}{N_i} = 49 \text{ db} - 20 \log_{10} 8 = 30.4 \text{ db.}$$

A slight improvement can be made by slightly over-modulating the tape recorder, according to a method described by Nichols and Rauch (1956). For overmodulation statistically 0.1% of the time, the improvement is 1.6 db. Hence, $\frac{S_i}{N_i} = 32$ db. Now to compute $\frac{S_o}{N_o}$ with $\beta = 10$.

$$\frac{S_o}{N_o} = \sqrt{3}\,(10)^{3/2}\,\frac{S_i}{N_i}$$

$$= 32 \text{ db} + 20 \log_{10} (3\times10^3)^{1/2} = 66 \text{ db.}$$

b. Frequency Modulation Noise (Wow and Flutter)

Speed variations of the tape recorder have a direct effect on the accuracy of the recorded data in FM systems because the speed variation acts as a multiplier of the recorded subcarrier frequency. The percentage magnitude of the error is given by:

$$E = \frac{f_c F}{B_c}$$

Where E = the percentage peak-to-peak error signal out of the

discriminator,

f_c = the subcarrier center frequency, and

F = the maximum percentage peak-to-peak flutter variation of the tape recorder.

It is readily apparent that for constant bandwidth systems the magnitude of the error signal increases to a maximum for the highest subcarrier frequency utilized. This error signal can be reduced by using tape-speed compensation to correct for the effects of speed variations in the tape recorder. By recording an unmodulated reference tone, the tape-speed error can be converted to a voltage at the output of a reference discriminator. This voltage is then applied to the tape-speed-compensation inputs of all data discriminators. To accomplish theoretically perfect performance, the compensation signal at the FM detector in the discriminator must be of the same amplitude and phase as the error signal. Since these parameters for both compensation signal and the data subcarrier signal are affected by filtering in all elements of the reduction system, perfect compensation is not realizable. The individual discriminator specifications show the practical improvement ratios attainable for various deviation ratios.

Using the above information, the signal-to-noise ratio due to flutter of the tape recorder can be written:

$$\frac{S_e}{N_o} = \frac{100\,R_t}{E} = \frac{100\,B_c\,R_t}{f_c\,F}$$

where S_o = the maximum rms output data signal,

N_o = the rms output noise due to flutter, and

R_t = the improvement ratio as given in the discriminator specifications.

The Ampex FR-1300 has a peak-t0-peak wow and flutter specification of 0.70% over a bandwidth of 1,250Hz. at 7.5 i.p.s. Using these numbers, and taking R_t = 40 db, we can determine the S/N ratio out of each subcarrier discriminator due to the tape flutter component. The narrowest deviation, or worst-case channel is 7.3 kHz. For this channel operated at a modulation index of 10, the signal-to-noise ratio is

$$\frac{S_o}{N_o} = \left(\frac{100}{0.70}\right)\left(\frac{5 \times 10^2}{7.3 \times 10^3}\right)(100) = 9.8 \times 10^2 = 60 \text{ db}$$

Table 5 shows the results of similar computations of FM noise at all six tape speeds, and for data channels of center frequencies 2kHz., 7kHz., and 14kHz. This improvement figure is conservative for three reasons: (1) the flutter value used in the computations was measured a 1,250 Hz. band, while the data bandwidth is only 25 Hz.; (2) the improvement ratio of 100 or 40 db is probably a conservative number; (3) the signal-to-noise ratio is considered RMS to RMS while the quantities we are dealing with here are specified in peak-to-peak numbers with no information furnished as to their spectral distribution. The corresponding S/N ratio for the 2.3 kHz $\pm$ 250 Hz and 13.3 kHz $\pm$ 250 Hz channels are,

respectively, 70 db and 54 db.

The EMR 4150 data discriminator specification guarantees 33 db of improvement when operating at MI =5. EMR engineers claim 40 db is an applicable figure to our system because we will operate at MI = 10. At low data frequencies, the improvement ratio increases linearly to greater than 46 db at DC. Therefore we might expect a broadband S/N ratio from wow and flutter of 60 db for the first six channels, and better at low data frequencies.

2. Dynamic Nonlinearity (Harmonic Distortion)

In general, the dynamic nonlinearity generated in an FM system is attributable to the amplitude and phase response of bandpass filters of the narrowest pass band which filter the modulated subcarrier signals. These are: (1) the discriminator input filter and (2) the VCO output filter. Dynamic distortion of the detected FM signal is caused by changes in the amplitude and phase of component in the modulated-carrier spectra. The distortion can be calculated from the components of the filtered spectrum through the use of a technique described by J. Schenck and W. F. Kennedy (1959).

EMR discriminators, when operated at MI = 2, give total harmonic distortion numbers that are less than 0.8% and typically about 0.6% at 1/3 the data cutoff frequency. When operated at MI = 10, the total harmonic distortion will be lessthan 0.5 when measured at 12.5 Hz or 1/2 the cutoff

frequency of the low pass filter. The total harmonic distortion figure will generally decrease in magnitude as we move away from 1/2 cutoff frequency in either direction.

3. Adjacent Channel Crosstalk

The sidebands of the adjacent FM subcarrier will produce crosstalk in each channel. The magnitude of this crosstalk is a function of channel spacing, deviation ratio, and the characteristics of both the discriminator bandpass input filter and lowpass output filter. The effect of the VCO output filter on this type of crosstalk generally is negligible. The output crosstalk of a subcarrier discriminator resulting from an interfering signal can be calculated using a method described by Arguimbau (1956).

$$\left.\begin{matrix}\text{fractional} \\ \\ \text{crosstalk}\end{matrix}\right\} = \left(\frac{f_c - f_i}{\Delta f}\right)(a \cos ft + a^2 \cos 2ft + a^3 \cos 3ft + \cdots)$$

where $f_c - f_i$ = frequency difference between the desired signal, f_c, and the interfering signal, f_i,

Δf = full-scale deviation, and

$$a = \frac{A_i}{A_c}$$

where A_i = amplitude of interfering signal, and

A_c = amplitude of desired signal.

All terms other than (a cos ft) represent crosstalk which is harmonically related to the fundamental beat frequency. In general, they are negligible due to output filtering. An

approximate expression of overall output crosstalk resulting from an adjacent channel for n significant sidebands can be written:

$$R^2 = \sum_n \left[\left(\frac{A_i}{A_c} \right) \left(\frac{f_c - f_i}{\Delta f} \right) \left(Y_{BPIF} \right) \left(Y_{OF} \right) \right]_n^2$$

where R = overall fractional rms crosstalk

$Y_{BPIF} = \dfrac{\text{attn. to } f_i}{\text{attn. to } f_c}$ of bandpass filter,

Y_{OF} = attn. to $(f_c - f_i)$ of output filter.

Considering the statistically deviated case where channel 1 (2.3 kHz.) is at the upper bandedge and channel 2 (3.3 kHz) is at the lower bandedge and the subcarrier amplitudes are equal, we have for the deviation ratio of 10 case

$$f_c - f_i = (3.05 \times 10^3) - (2.55 \times 10^3) = 0.50 \times 10^3$$

$$\Delta f = 0.25 \times 10^3$$

$$Y_{BPIF} = \frac{3 \text{ db}}{25 \text{ db}} = -22 \text{ db} = 0.08$$

$$Y_{OF} = 0.4 \times 10^{-4} + 30 \text{ db} = 1.3 \times 10^{-3}$$

$$R = \frac{A_i}{A_c} \frac{f_c - f_i}{\Delta f} Y_{BPIF} Y_{OF}$$

$$R = 1 \frac{0.5 \times 10^3}{0.25 \times 10^3} (0.08)(1.3 \times 10^{-3})$$

$$= 86 \text{ db}$$

The total crosstalk generated by more than one signal interfering channel can be calculated by taking the square root of the squares of each error component that is calculated.

E. Telemetry System Performance

Measurements of noise and crosstalk were made on selected channels in the telemetry system. Noise from the B-filter channels was measured at the output of the discriminator from a tape made at 3 3/4 inches per second. The filter input was a resistance equivalent to the accelerometer impedance. The measured peak-to-peak noise was 10 millivolts, referred to 5 volts peak-to-peak full scale signal output, corresponding to a signal to noise ratio of 54 db. The system specification for this ratio at 3 3/4 i.p.s. lies between 56 db and 63 db., depending on the channel. No difference in the measured noise among the channels was observed.

Crosstalk was measured between B-filter channels by applying to one channel a sine wave input at 10 Hz. and 20 Hz. which gave outputs of 4 volts peak to peak. The outputs of the other channels, whose inputs were grounded, were examined for any signal at the test frequency. A 6 db improvement was made over the signal to noise ratio by visually filtering the output noise. No test signal could be seen. Hence, the inter-channel separation at 10 Hz. and 20 Hz. in the B-filter channels is determined to be greater than 60 db. The system specification is 86 db.

Records of the outputs of the low frequency A-filter channels during the experiment are shown in Figures 16 through 18. These records were made with the accelerometers running, and in place at sites 1,2 and 3. Hence, they show telemetry system noise along with accelerometer noise, seismic noise, and, if any, seismic signals from the experiment. Apparently, the transverse component of Remote Data Station 2 was not working. Also, we note that the longitudinal component of Remote Data Station 1 developed an instability during the day, but operated normally at night. Figure 18 shows that both working channels of Remote Data Station 2 were very noisy. This station was at site 1, and the nearby air compressor may have contributed to this noise. The noises from Remote Data Station 1 and the Local Data Station are summarized in Table 6.

EXPERIMENT

A. General Description

The experiment had two purposes. First, it served as a test of the accelerometer telemetry system in an actual field situation. Although the radio links in the system were not used (hard wire telemetry was appropriate to the short distances) the rest of the system was tested under environmental conditions similar to those for which it was intended. Secondly, the experiment made possible a study of the seismic near field of the air gun.

The air gun used was the PAR Model 600B, manufactured by Bolt Associates, Inc. The gun is basically cylindrical, with diameter 15 cm and length 46 cm. Described fully by Luskin (1970), the air gun creates an acoustic pulse output by the explosive release of high pressure air into the surrounding water. An air chamber of 40 in^3 was used with air pressurized to 2000 psi. The manufacturer specifies the peak output pressure under these conditions at a distance of 1 yard to be 2 bar. A gasoline powered air compressor supplied the pressurized air. The gun was fired every 6 seconds (later increased to every 10 seconds) by an automatic trigger. The gun was operated in a hole in an area of flat, hard granite. The hole, which was cut to our specifications, is cylindrical, 175 cm diameter and 165 cm deep. The gun was held in place in the center of the hole by a metal rig which attached with rock anchors at three places on the side of the hole, and at the bottom. During the experiment, the hole was filled with water, and water lost due to splashes was replaced from time to time.

The site of the experiment is an operating granite quarry in North Chelmsford, Massachusetts. The area surrounding the source hole and all the accelerometer sites consists of relatively unweathered, hard granite. About 15 m southwest of the hole (Figure 19) is a sheer cliff which drops to the main cut of the quarry. About 10 m northwest of the hole

is a straight, vertical cliff rising 5 m above the hole (Figure 20). The lower surface (near the hole) and the upper surface (northwest of the cliff) are both horizontal, flat rock. The pond shown in Figure 19 is less than 1 m deep.

The accelerometer packages were attached to the granite surface with plaster of Paris. All the accelerometer packages were aligned such that the longitudinally sensitive axis pointed toward the hole. The sensors at sites 1 and 2 remained there throughout the experiment. The third sensor was first set up at site 3, and later moved to site 4. As seen in Figure 19, azimuthal coverage of about 180 degrees about the source was obtained. There was no convenient rock exposure to the southeast of the source to allow for a site there.

B. P Wave Amplitudes

Two theoretical models were considered in attempting to predict the P wave amplitudes from the air gun shots. Heelan (1952) treats the problem of a uniform stress applied to the walls of an empty cylindrical cavity in a homogeneous, infinite medium. He computes the radiated P, SV and SH waves from the source for distances from the source large compared to the wavelength, and neglects the near field terms. Since in our experiment all the sensors were placed much less than 1 wavelength from the source, where the near field terms exist together with the radiated waves, we would expect Heelan's estimate to be considerably smaller than the

measured amplitude. Heelan's result for the radial displacement produced by a pressure transient $p_o\, g(t)$ is

$$u_r(t) = \frac{a^2 d \rho_o}{4 \mu \alpha r}\left[1 - 2\frac{\beta^2}{\alpha^2}\cos^2\phi\right] g'\left(t - \frac{r}{\alpha}\right)$$

where

a = hole radius = 87.5 cm

d = hole depth = 165 cm

μ = shear rigidity $\approx$ 1.8×10^{11} dyne-cm^{-2}

α = compressional velocity $\approx 5.5 \times 10^5$ cm-sec^{-1}

β = shear velocity $\approx 3.0 \times 10^5$ cm-sec^{-1}

r = distance

ϕ = ray angle from veritcal

p_o = peak source pressure = 2×10^6 dyne-cm^{-2}

$g(t)$ = dimensionless source time dependance.

Assuming $\phi \approx 60^\circ$, and that $g(t)$ has a rise time of 8 msec., as evidenced by Kramer, et al., (1968), we find the predicted amplitudes shown in Table 7. These results must be considered as a lower estimate of the expected amplitudes.

Sharpe (1942) treats the related problem of finding the elastic displacements caused by a pressure transient applied to the wall of a spherical cavity in a homogeneous, infinite medium. His solution applies to the near field as well as the far field. We can use Sharpe's analysis if we equate the radius of our cylindrical hole with the radius of Sharpe's equivalent spherical cavity, and if we multiply the resultant amplitudes by a factor of 2 to approximately correct

for the effect of the free surface. We first consider the displacement function $u(\tau)$ produced by a source stress function of the form

$$p(t) = \begin{cases} p_o & t \geq 0 \\ 0 & t < 0 \end{cases}$$

Then, modifying Sharpe's result as described above, we get

$$u(\tau) = \begin{cases} \frac{a^2 p_o}{\sqrt{2}\mu r} e^{-\omega\tau/\sqrt{2}} \sin \omega\tau, & \tau \geq 0 \\ 0, & \tau < 0 \end{cases}$$

where

a = radius of spherical cavity

p_o = peak source pressure

μ = shear rigidity

r = distance from the source

$\tau \equiv t - \left(\frac{r-a}{v}\right)$

v = compressional velocity

$\omega = \frac{2\sqrt{2}\, v}{3a}$

Evaluation of the amplitude coefficients

$$x_i \equiv \frac{a^2 p_o}{\sqrt{2}\mu r_i}$$

above, using the values $\mu = 1.8 \times 10^{11}$ dyne-cm^{-2}, $a =$ 87.5 cm., $p_o = 2 \times 10^6$ dyne-cm^{-2}, $r_1 = 8.8 \times 10^2$ cm,

$r_2 = 2.1 \times 10^3$ cm, $r_3 = 1.3 \times 10^3$ cm, $r_4 = 1.6 \times 10^4$ cm yields

$x_1 = 6.8 \times 10^{-5}$ cm (site 1)

$x_2 = 2.9 \times 10^{-5}$ cm (site 2)

$x_3 = 4.6 \times 10^{-5}$ cm (site 3)

$x_4 = 3.8 \times 10^{-5}$ cm (site 4)

Sharpe obtains the displacement functions for realistic stress time functions from the above step function solution by using Duhamel's integral. We can use the result for a stress function of the form

$$p(t) = \begin{cases} p_0 e^{-t/\tau}, & t \geq 0 \\ 0, & t < 0 \end{cases}$$

Measurements reported by Kramer, et al. (1968) of the pressure in the water at a distance of 3 feet from a shallow air gun suggest this functional form of the stress. The peak displacements for this source function are shown in Table 7, along with the predictions by Heelan, and the observed data.

C. Azimuthal Dependance of SH Waves

The simplest theory to describe the air gun source is one in which the hole is a perfect cylinder, the pressure wave from the gun is symmetrical, and the gun is mounted on the center line of the hole. From such an ideal source we would expect no transverse (SH) components of motion. Although mode conversion by heterogeneities in the rock could account for SH waves in the far field, observations within less than

one quarter wavelength from the source must be considered to be free from this effect.

The next simplest theory would be to consider the source as the superposition of a symmetric and a dipole source. The motivation for this theory comes from considering the effect if the air gun were placed slightly eccentrically in the hole. We may predict the SH radiation pattern from only the strength and orientation of the dipole. Conversely, we may determine the closeness of fit the observed data make with a dipole pattern; and the orientation of the dipole by considering only the relative amplitudes of the SH motion. SH accelerations from all four stations were measured. At each station, the sense and average amplitude of transverse motions from a large number of shots was calculated. In order to study the SH amplitudes from different stations with respect to azimuth, the effect of distance on the amplitudes must be removed. The SH amplitudes were normalized as follows:

$$a^*_{SH} = \frac{a_{SH}}{(a_L^2 + a_V^2)^{1/2}}$$

where a^*_{SH} is the normalized SH amplitude, and a_{SH}, a_L and a_V are respectively the average measured transverse, longitudinal and vertical amplitudes. The normalized SH amplitudes are listed in Table 8. The radiation pattern from a dipole

has angular dependence proportional to sin θ when θ is measured from the dipole axis. Figure 21 shows the normalized SH amplitudes plotted against azimuth about the source. Zero degrees refers to the direction from the source to site 1. A segment of a sine curve is drawn on the graph to best fit these data to a dipole pattern. This pattern represents a dipole component with nodal line between sites 1 and 4, 50 degrees from site 1, shown in Figure 19.

Another possible source of the SH waves comes from the possible asymmetry of the source itself. Unfortunately, we don't know how symmetric the main pressure pulses from the air gun actually were. An air gun is usually described as a spherically symmetric source. But tests are usually carried out in deep water with the sensors more than 10 m from the gun. In our experiment, the gun was shallow, and the rock wall was within less than 1 m from the gun. If the air were released asymmetrically from the ports, creating lateral pressure inhomogeneities in the wave, these inhomogeneities would normally (if the wave travelled long enough in water) have time to equilibrate as the wave expanded. But in a bore hole such as we used, these inhomogeneities may not have had time to die out before striking the wall and generating shear waves.

D. Suspension Failure

Thirty-one hours after the experiment began, the metal rig which held the air gun in place in the hole broke loose

from the rock. The failure was discovered when the bubbles from the shots were seen to be rising from an unusual place in the hole. When the water was pumped out, the gun was found lying on the bottom of the hole. Exactly how long it had been operating like that was unknown at that time. A plot of the accelerometer records at sites 1, 2 and 3 during that period is shown in Figure 22. The time at which the tape recorder was stopped is marked "A". Most of the records show a noticeable change in amplitude at the time marked "B", about 3.8 minutes before "A". We believe this is when the suspension broke. A new suspension was improvised, and the experiment resumed. From this time on, the air gun firing interval was changed from 6 to 10 seconds. Apparently changing the suspension caused no significant change in amplitudes.

E. Amplitude Variations from Shot to Shot

Amplitude variations of 20 to 50 per cent both before and after the suspension change are observed from shot to shot at all stations, and in all components (Figure 22). This effect is thought to be caused by some change in the source, rather than in the rock or sensors. One possible cause is variations in the rate and direction of the released air from the gun. This behavior, if it occured, may be normal for this type of air gun, or it may have been induced by turbulence in the water at the onset of each shot. The manufacturer of the gun can recall no similar

amplitude fluctuations, suggesting that our application in the small shallow hole plays a part. Another possible cause might be variations, if any, in the pressure of the air supplied to the gun. However, although shot energy is directly proportional to the air pressure, it is considered unlikely that such large pressure variations actually occured. One further possibility is the perturbation of the expanding shock wave by the air remaining in the water from the preceding shot. The released air bubble had a volume of 40 in^3 at a pressure of 2000 psi, which corresponds to 6×10^3 in^3 at atmospheric pressure, or a sphere of radius 11 inches. After each shot, water in the hole was set into violent turbulence which did not subside by the time of the next shot. Furthermore, air from the preceding shot was typically still rising in the form of froth at the time of each shot. Such an air-water suspension could conceivably cause distortion of the pressure wavefront sufficient to partially destroy its coherence upon hitting the rock boundary, which in turn would modify the wave shape and amplitude recorded.

CONCLUSIONS

1. The telemetry system appears to have worked properly. The malfunctioning of one low frequency channel, and the unstable behavior of another during the day still must be explained. But the system's performance in a field situation was basically satisfactory.

2. Amplitudes from the air gun may be predicted with reasonable accuracy by Sharpe's explosion model. Heelan's model, although more suited to the shape of the source, neglects the near field terms and is, therefore, not appropriate at the distances observed.

3. SH waves are generated by the air gun source. Observations at various azimuths indicate a nodal line of SH motion. The SH waves may be caused by an off-center source, or by an asymmetric release of air from the gun. The last possibility could be determined by repeating the experiment, recording the pressure in the water, at several points adjacent to the hole boundary.

ACKNOWLEDGEMENTS

The author is grateful to Professor Keiiti Aki, who first suggested developing the seismic telemetry system, for his constant help and direction in carrying out the experiment described and supervising the writing of this thesis. We wish to thank Mr. John LeMasurier for allowing us the use of his quarry, and for his kind assistance throughout the experiment. We also thank Mr. Paul Chelminski of Bolt Associates, Inc., for his technical help in operating the air gun. This work was supported by the Advanced Research Projects Agency, monitored by the Air Force Office of Scientific Research under contract number F44620-70-C-0103.

REFERENCES

Argiumbau, L. B., (1956). Vacuum Tube Circuits and Transistors, John Wiley and Sons, New York.

EMR Telemetry, Inc., (1970). "Technical Proposal for Seismic Research Data Acquisition and Reduction System", Proposal No. 032037.

Heelan, P. A.,(1953). Radiation from a Cylindrical Source of Finite Length , Geophys., 18, 685-696.

Kramer, F.S., Peterson, R. A. and Walter, W.C., eds.,(1968). Seismic Energy Sources 1968 Handbook, United Geophysical Corporation.

Luskin, B., (1970). The PAR Air Gun, paper presented before the 16th Annual Exploration Meeting of the Permian Basin Geophysical Society at Midland, Texas, on May 8, 1970.

Nichols, M. H. and Rauch, L. L., (1956). Radio Telemetry, Second Edition, John Wiley and Sons, New York.

Schenck, J., and Kennedy, W. F., (1959). Analysis of Multiplex Errors in FM/FM and PAM/FM/FM Telemetry, IRE Trans. on Space Electronics and Telemetry, SET-5, 138-147.

Sharpe, J. A., (1942). The Production of Elastic Waves by Explosion Pressures. Part I. Theory and Empirical Field Observations, Geophys. 7, 144-154.

White, J. E., (1965). Seismic Waves: Radiation, Transmission and Attenuation, McGraw-Hill, New York.

Table 1

A - Filter Electrical Characteristics

Input impedance = 1 megohm, minimum.

Output impedance = 5k.

1st Stage - gain = 500

1-pole high-pass at .0057 Hz. determined by R9, C9.

2-pole low-pass at .01 Hz. determined by R8, C8 and R2,C2.

1-pole high-pass at .01 Hz. determined by R1, C1.

1-pole low-pass at 1 kHz. determined by R,C.

2nd Stage - gain = 33.33

1-pole high-pass at .001 Hz. determined by R4, C3.

3rd Stage - gain = 2

1-pole high-pass at .001 Hz. determined by R5, C4.

1-pole low-pass at 10Hz. determined by R7, C5.

Table 2

B - Filter Electrical Characteristics

Maximum input voltage = ±10 volts

Input impedance = 6 megohm (minimum)

Output impedance = 5 k.

Low-cut frequency (determined by R1, C1) = .025 Hz.

Passband gain (determined by R2, R3) = 1/3

High-cut frequency (determined by R, C) = 25 Hz.

High-cut response = third order Butterworth

System response:

$$e_{out} = -e_{in}\left(\frac{R_1C_1p}{1 + R_1C_1p}\right)\left(\frac{1}{(1+RCp)[(1+RCp + (RCp)^2]}\right)\left(\frac{R_3}{R_2 + R_3}\right)$$

Table 3

Characteristics of FM Radio Link

Transmitters	Conic CTM-405K
Power Output	5 Watts
Receivers	Conic CAR-210
Receiver Sensitivity	5 microvolts (20 db S+N/N)
Frequencies	377.5 MHz. 391.5 MHz.
Bandwith	234 kHz.
Transmitting Antennas	Decibel Products DB-402 6 db forward gain
Receiving Antenna	Decibel Products DB-404SP Omnidirectional
Polarization	Vertical

Table 4

R.F. Power Computation

The following computation shows that at the rated range of 10 miles, the r.f. link has a power safety margin of 29 db. Not included in the computation are transmission line mis-matches and attenuation and propagation path attenuation. Hence, the safety margin will be smaller than 29 db.

Transmitter power (5 watts)	+35 dbm
Transmitting antenna gain	+ 6 db
Receiving antenna gain	+ 4 db
Free-space transmission loss over 10 miles	-109 db
Power delivered to receiver	-64 dbm
Power needed at receiver for 20 db quieting	-93 dbm
Power safety margin	29 db

Table 5

Tape Speed i.p.s	% Flutter peak to peak	$\frac{S_o}{N_o}$, f_c=2kHz.	$\frac{S_o}{N_o}$, f_c=7kHz.	$\frac{S_o}{N_o}$, f_c=10kHz.	$\frac{S_o}{N_o}$, f_c=14kHz
1 7/8	1.4	65 db	54 db	51 db	48 db
3 3/4	1.0	68	57	54	51
7 1/2	.70	71	60	57	54
15	.45	75	64	61	58
30	.40	76	65	62	59
60	.35	77	66	63	60

Table 6

	Record Amplitude millivolts, peak-to-peak	S/N ratio db
Local Data Station		
LA Day	60	38
LA Night	30	44
TA Day	140	31
TA Night	80	36
VA Day	120	33
VA Night	120	33
Remote Station 1		
LA Day	-	
LA Night	80	36
TA Day	100	34
TA Night	80	36
VA Day	120	33
VA Night	80	36

Table 7

Predicted and Observed Amplitudes

Site	Distance from Source (m)	Amplitude Predicted by Heelan ($\times 10^{-7}$ cm)	Amplitude Predicted by Sharpe ($\times 10^{-5}$ cm)	Observed L-Amplitude ($\times 10^{-5}$ cm)
1	8.8	8.8	2.0	11
2	21	3.7	.87	4.0
3	13	5.9	1.4	6.8
4	16	4.8	1.1	4.5

Table 8

SH Wave Amplitudes

Site	SH observed (gal)	$L^2 + V^2$ (gal)	SH normalized	Relative Azimuth (ref. site 1)
1	-4.4±.8	3.3±3.2	-1.3±.24	0
2	1.6±.7	.86±.7	1.9±.8	169°
3	.4±.2	2.1±1.6	.2±.1	115°
4	.86±.7	1.1±.4	.8±.6	73°

FIGURE CAPTIONS

1. Local data station set-up
2. Remote data station set-up
3. Local data station
4. Remote data station
5. Telemetry system block diagram
6. Local data station block diagram
7. Remote data station block diagram
8. Recording and discriminating system block diagram
9. A-filter response
10. B-filter response
11. A-filter full scale ground displacement
12. B-filter full scale ground acceleration
13. A-filter schematic diagram
14. B-filter schematic diagram
15. Power supply block diagram
16. Local data station (site 2) A-filter records. Longitudinal (LA), Transverse (TA) and Vertical (VA) records for day and night. Numbers in parentheses are reciprocal of sensitivity in millivolts per small division. Time scale is 1 minute per division.
17. Remote data station 1 (site 3) A-filter records. Longitudinal (LA), Transverse (TA) and Vertical (VA) records for day and night. Numbers in parentheses are reciprocal of sensitivity in millivolts per small division. Time scale is 1 minute per division.
18. Remote data station 2 (site 1) A-filter records. Longitudinal (LA), Transverse (TA) and Vertical (VA) records

for day and night. Numbers in parentheses are reciprocal of sensitivity in millivolts per small division. Time scale is 1 minute per division.

19. Map of experiment area

20. Cross-sections showing spatial relations among hole, cliff and site for sites 2, 3 and 4. Dimensions are in meters.

21. Azimuthal plot of corrected SH amplitudes. Suggested sine-θ dependance is drawn for reference.

22. B-filter accelerometer records at sites 1, 2 and 3 during suspension failure.

Figure 1

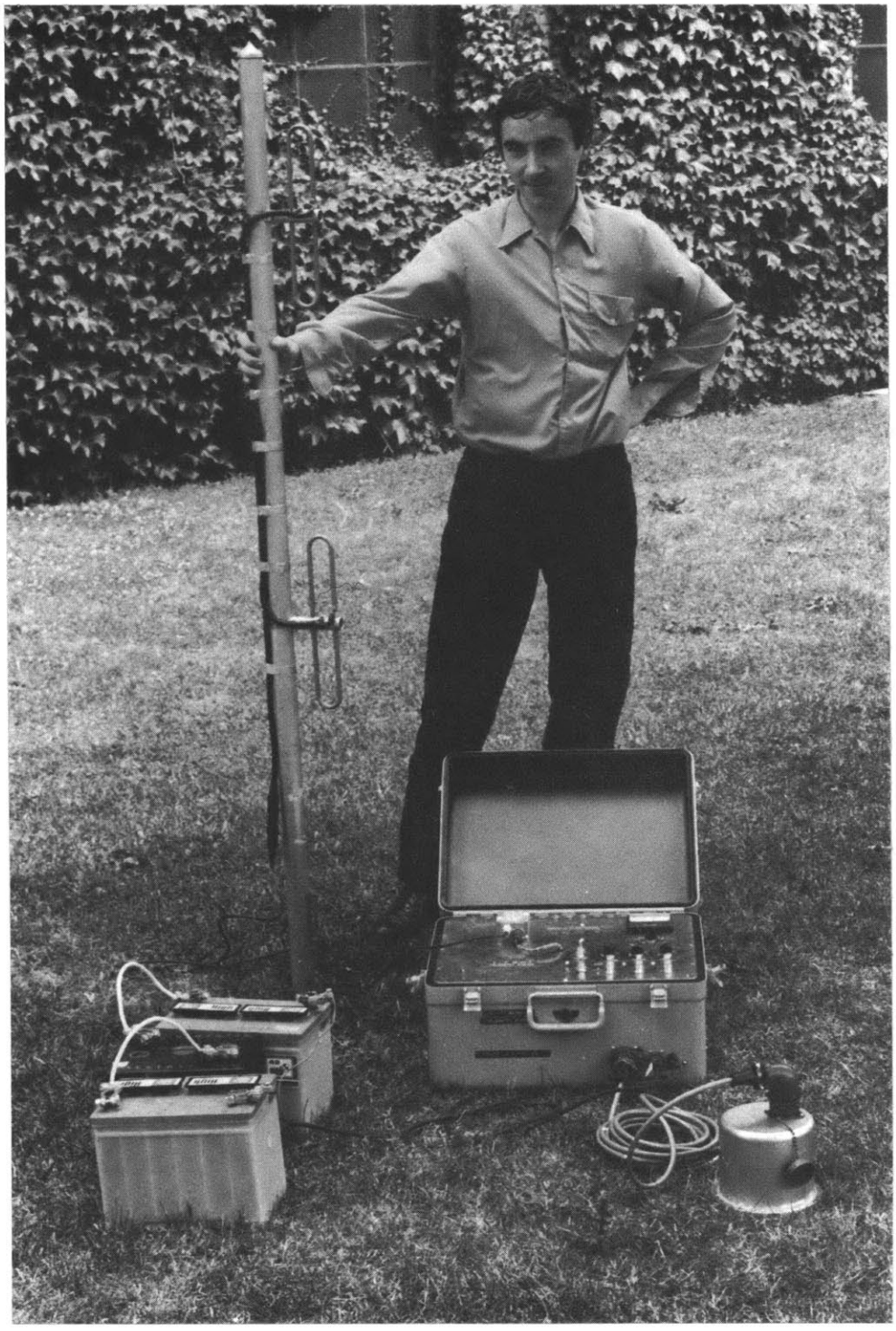

Figure 2

Figure 3

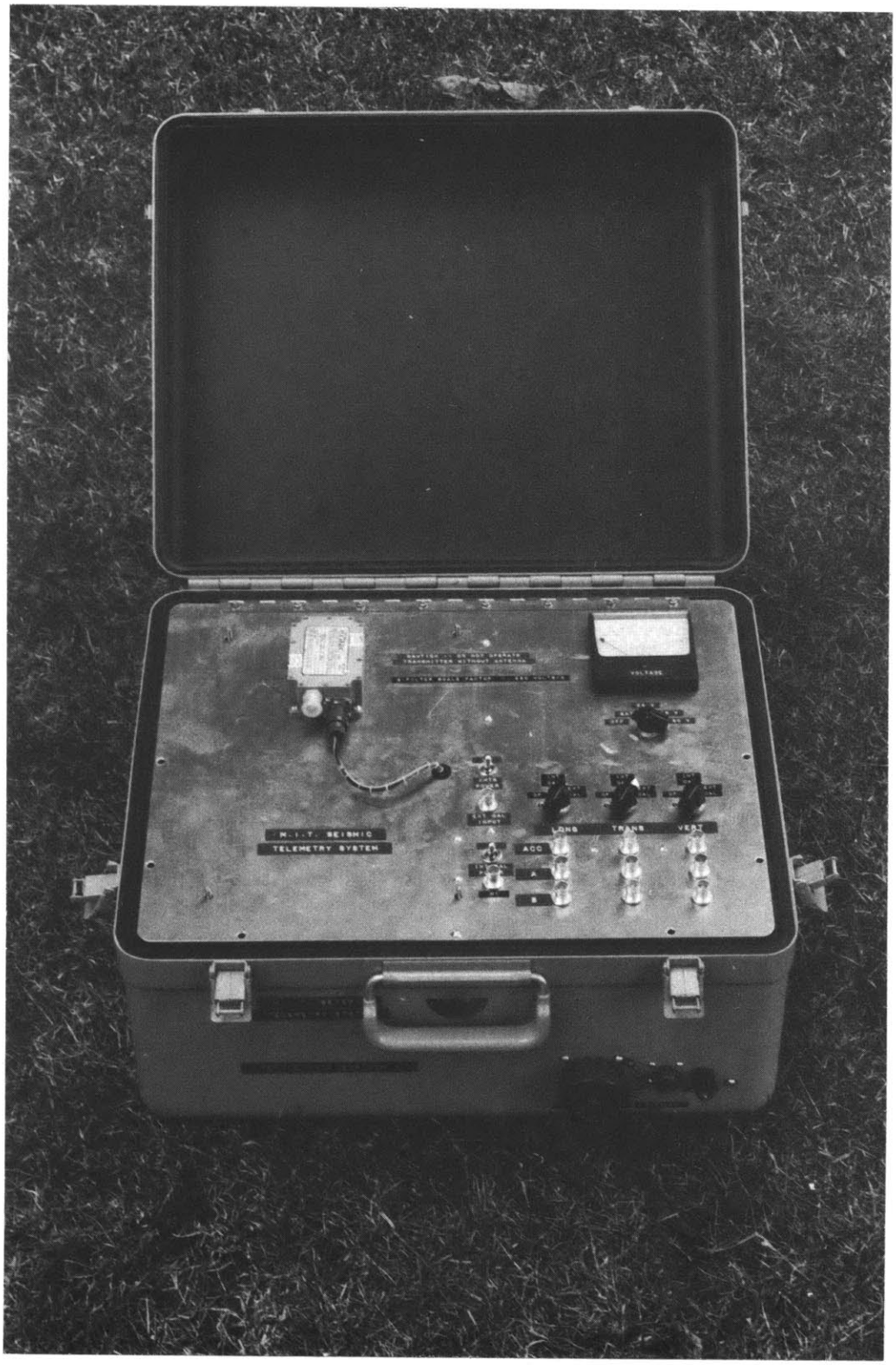

Figure 4

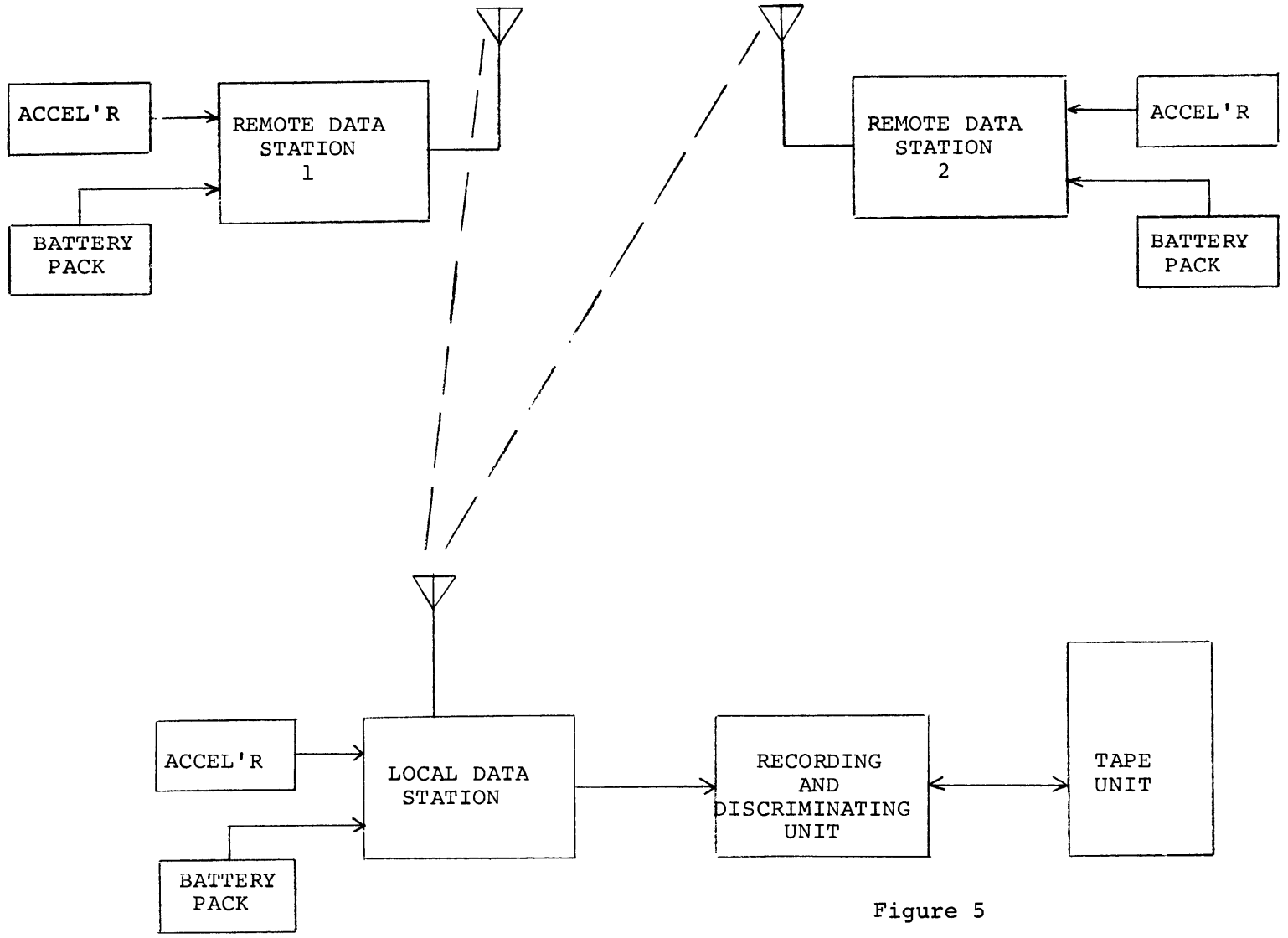
ACCEL'R
REMOTE DATA STATION 1
BATTERY PACK
REMOTE DATA STATION 2
ACCEL'R
BATTERY PACK
ACCEL'R
LOCAL DATA STATION
BATTERY PACK
RECORDING AND DISCRIMINATING UNIT
TAPE UNIT

Figure 5

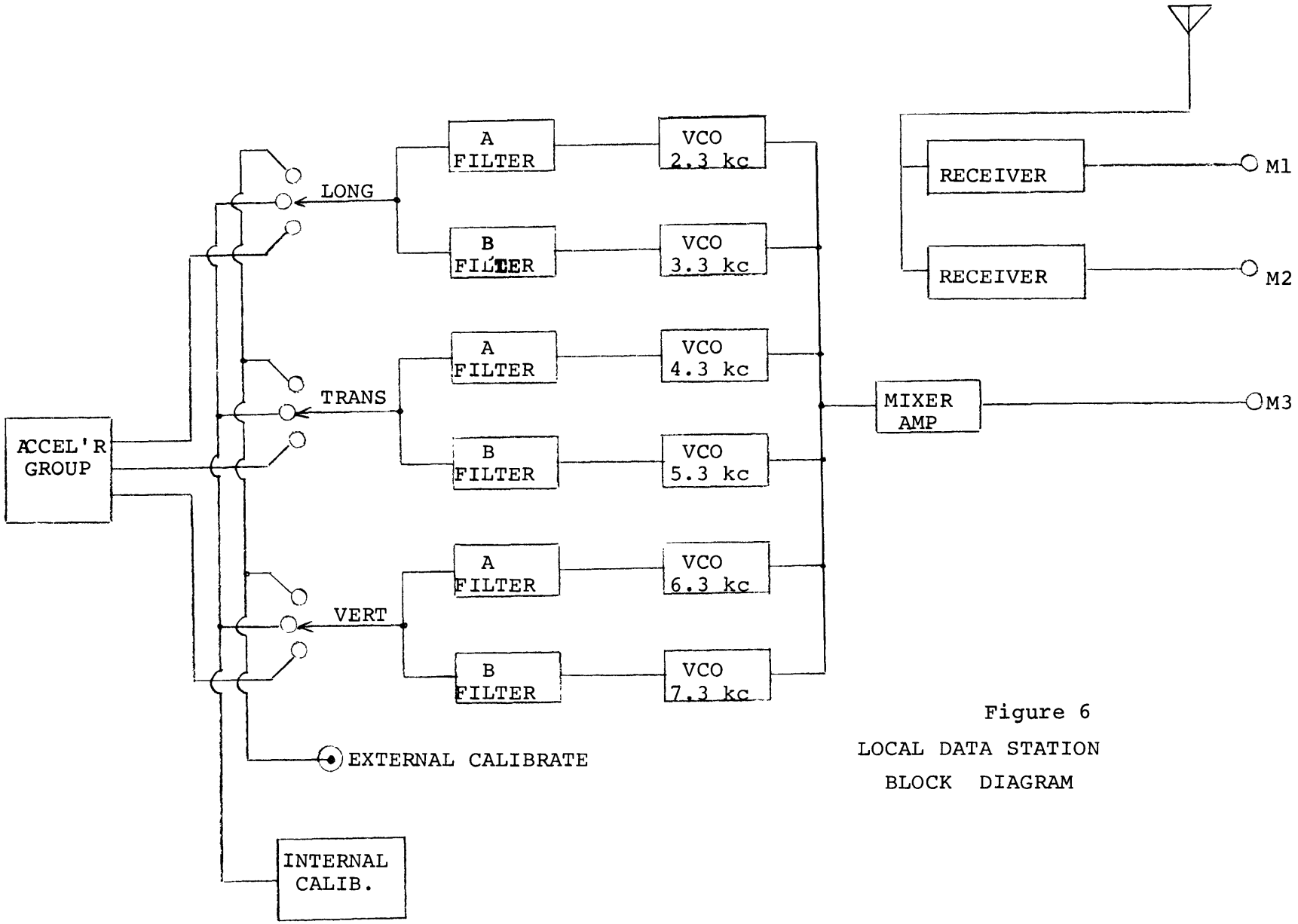

Figure 6

LOCAL DATA STATION

BLOCK DIAGRAM

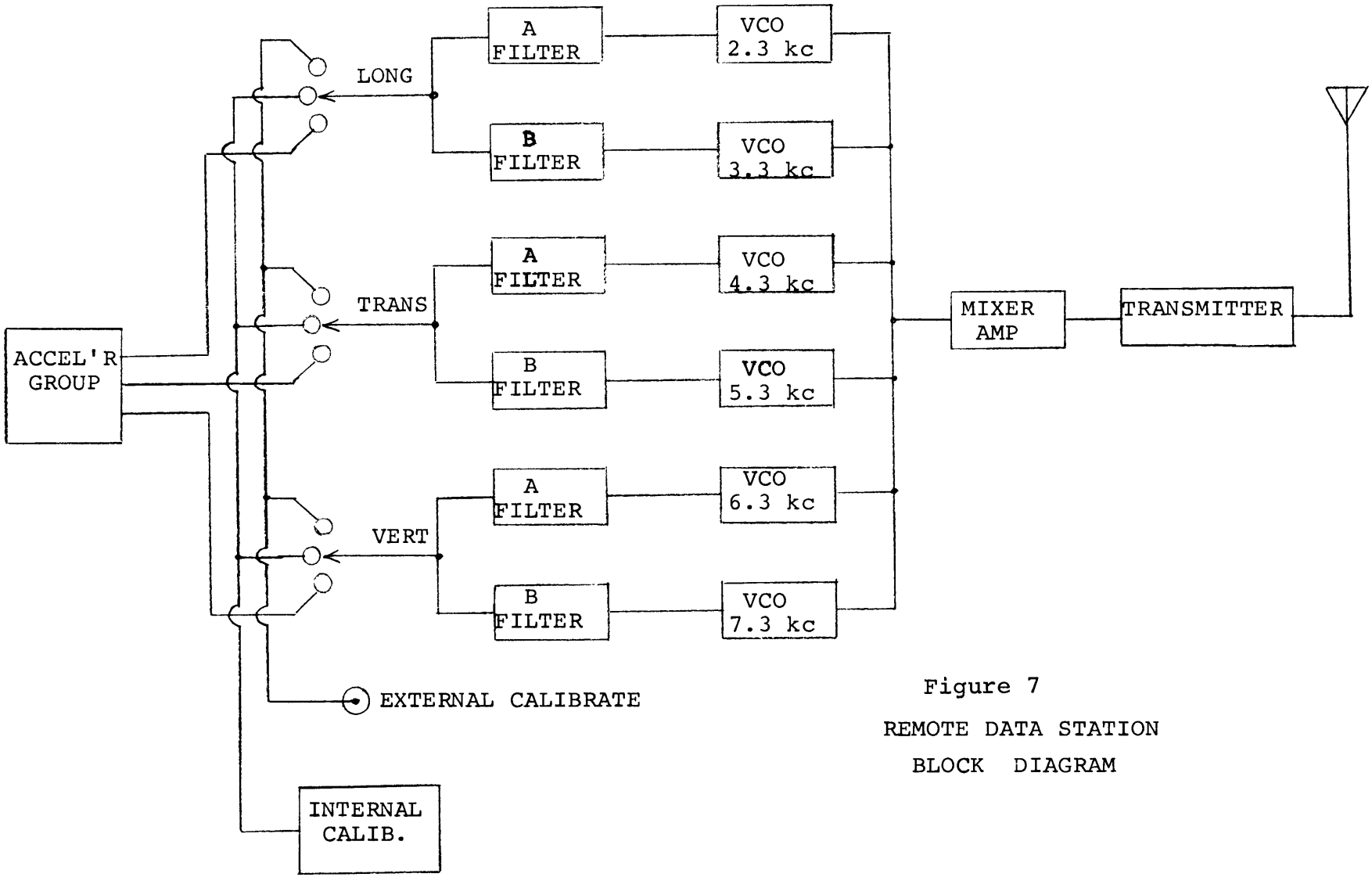

Figure 7

REMOTE DATA STATION

BLOCK DIAGRAM

RECORDING AND DISCRIMINATING SYSTEM

BLOCK DIAGRAM

Figure 8

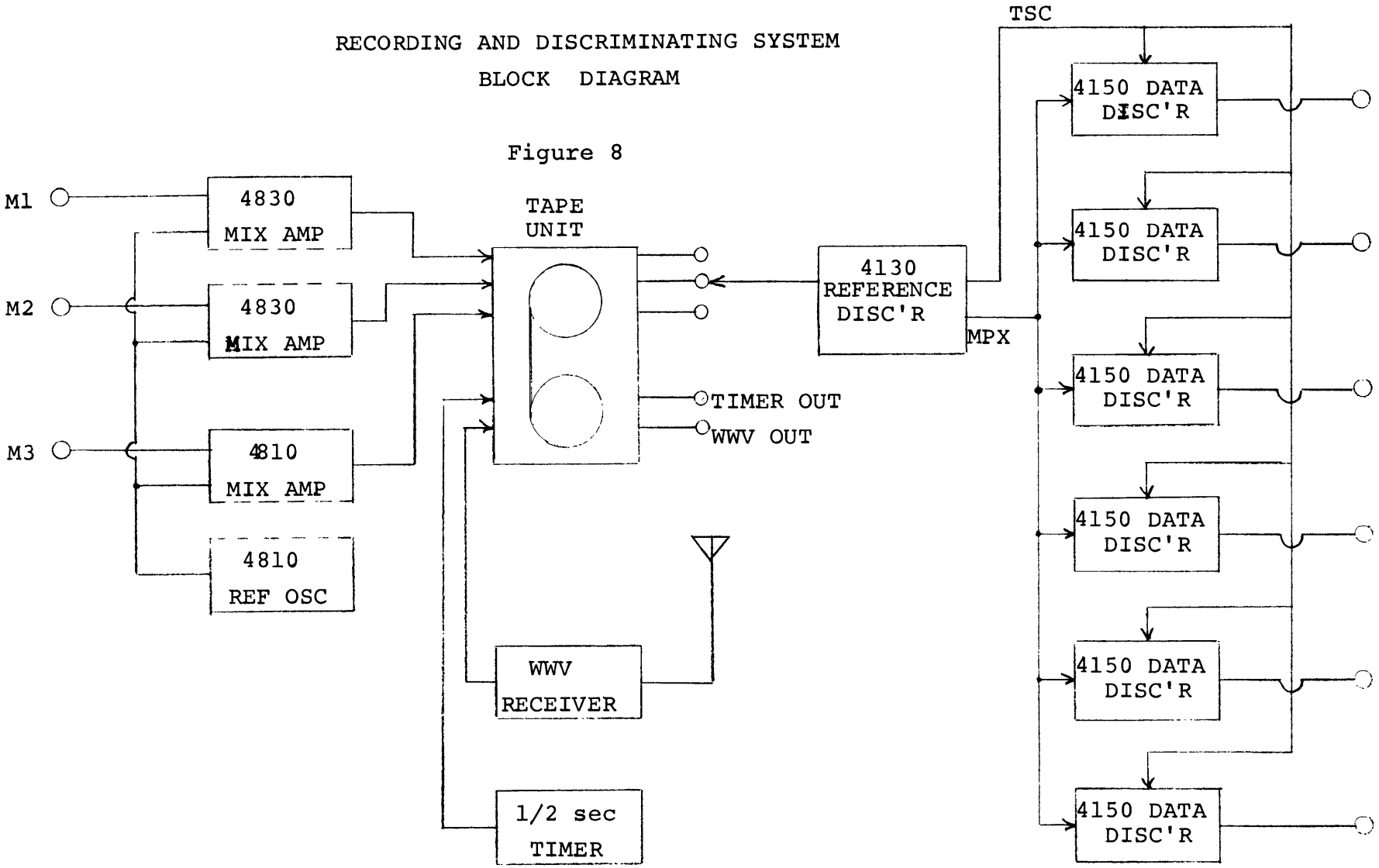

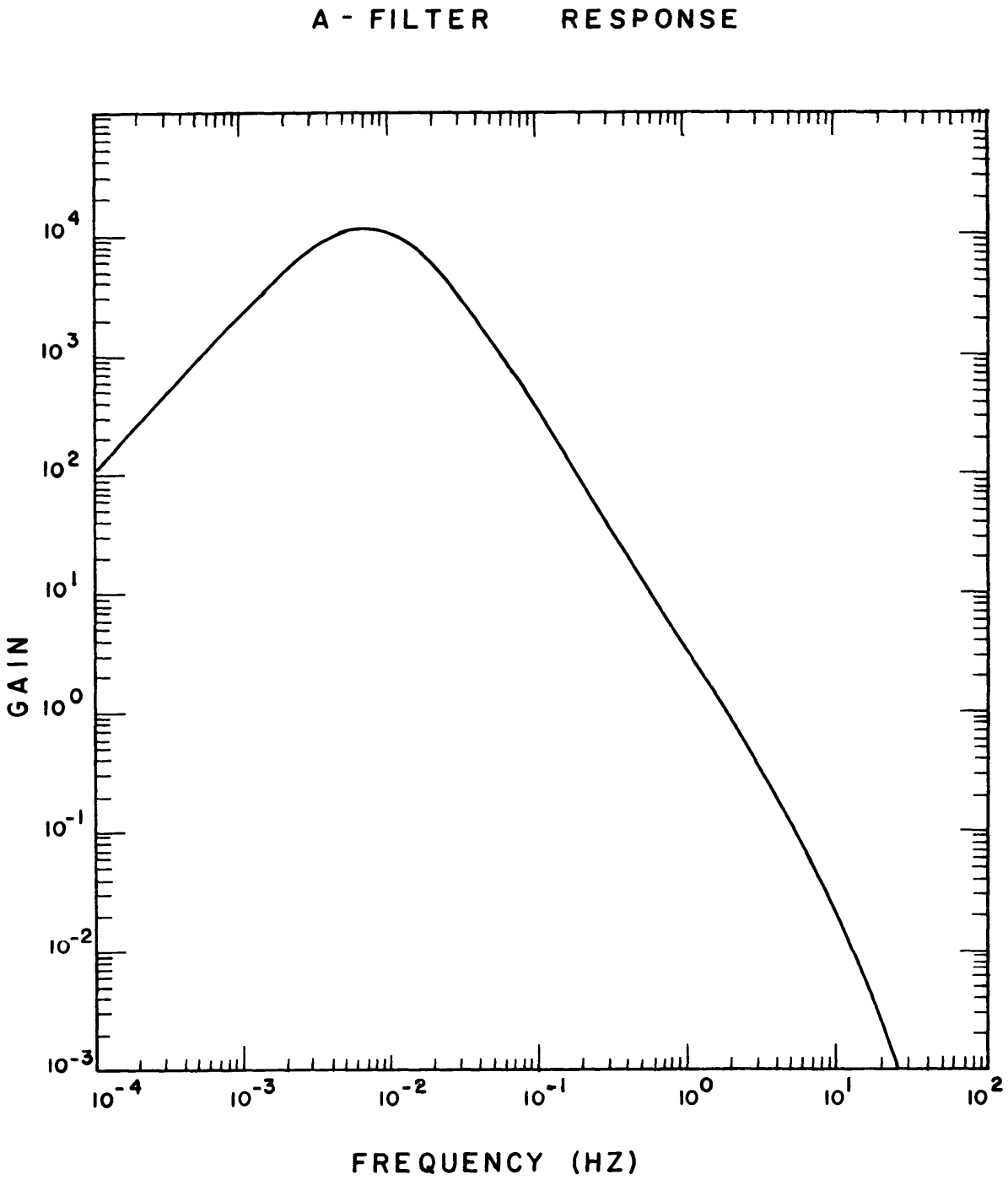
A - FILTER RESPONSE
GAIN
10^{4}
10^{3}
10^{2}
10^{1}
10^{0}
10^{-1}
10^{-2}
10^{-3}
10^{-4}
10^{-3}
10^{-2}
10^{-1}
10^{0}
10^{1}
10^{2}
FREQUENCY (HZ)

Figure 9

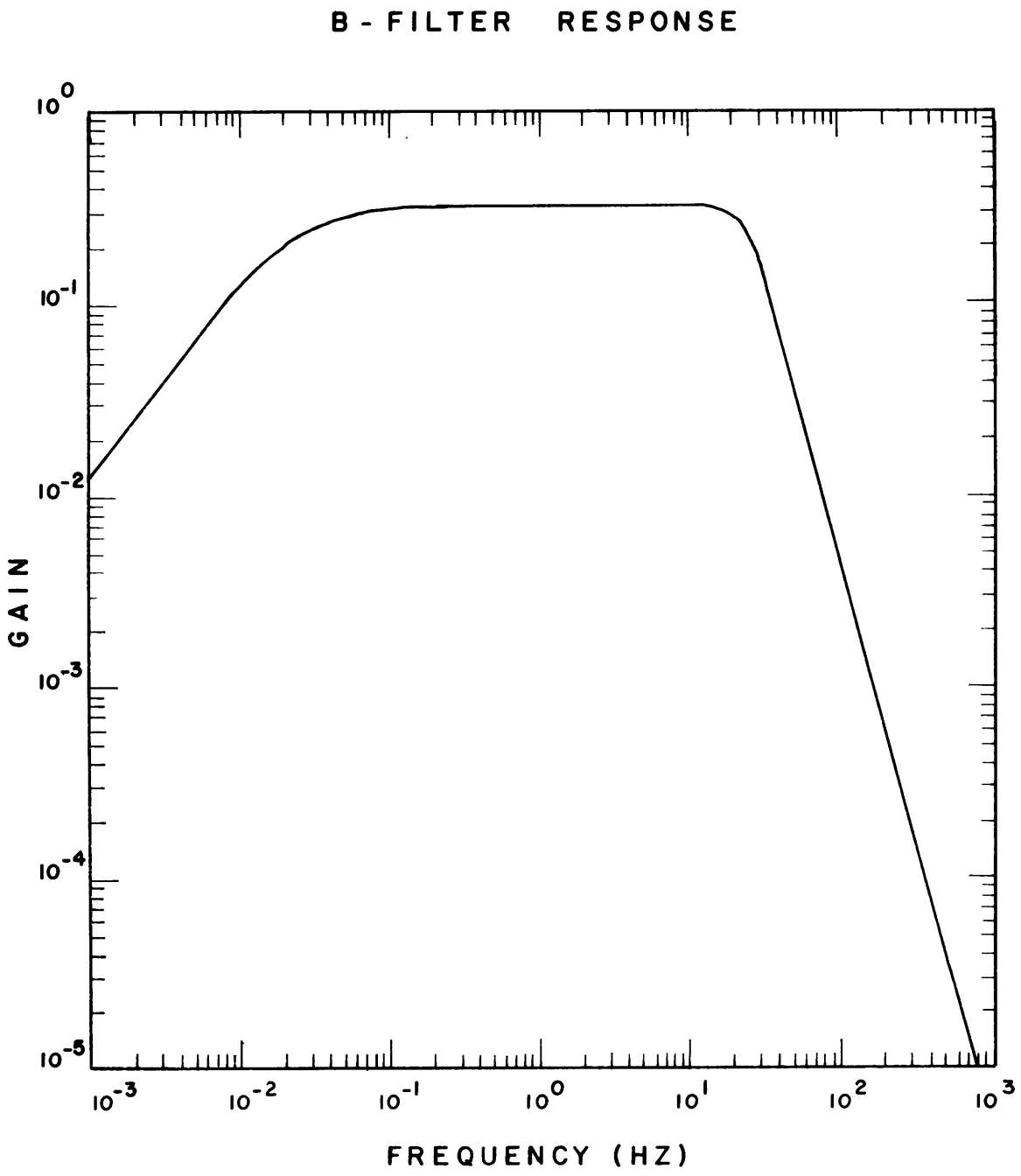
B - FILTER RESPONSE
GAIN
10^{0}
10^{-1}
10^{-2}
10^{-3}
10^{-4}
10^{-5}
10^{-3}
10^{-2}
10^{-1}
10^{0}
10^{1}
10^{2}
10^{3}
FREQUENCY (HZ)

Figure 10

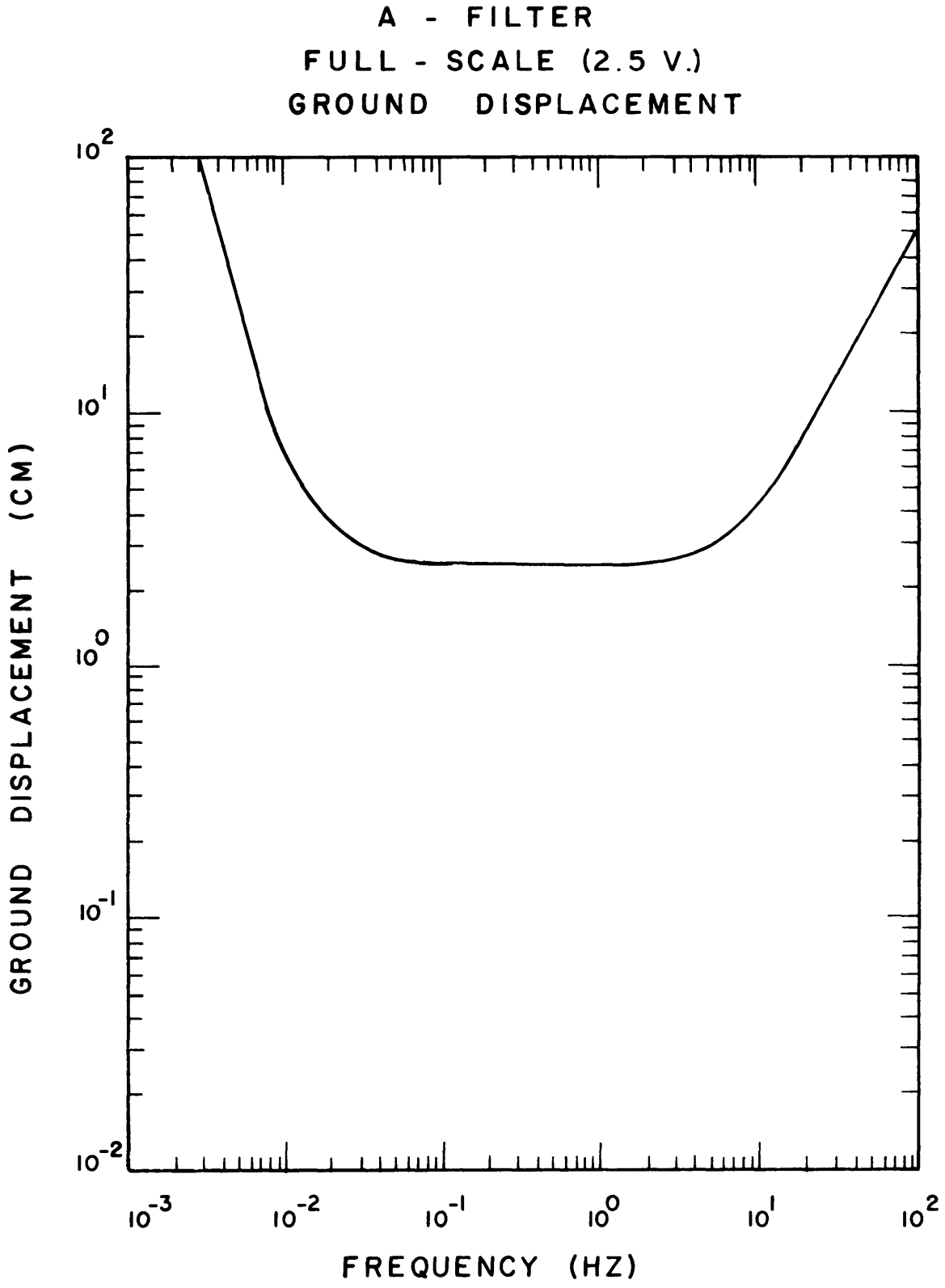
A - FILTER
FULL - SCALE (2.5 V.)
GROUND DISPLACEMENT
GROUND DISPLACEMENT (CM)
10^{2}
10^{1}
10^{0}
10^{-1}
10^{-2}
10^{-3}
10^{-2}
10^{-1}
10^{0}
10^{1}
10^{2}
FREQUENCY (HZ)

Figure 11

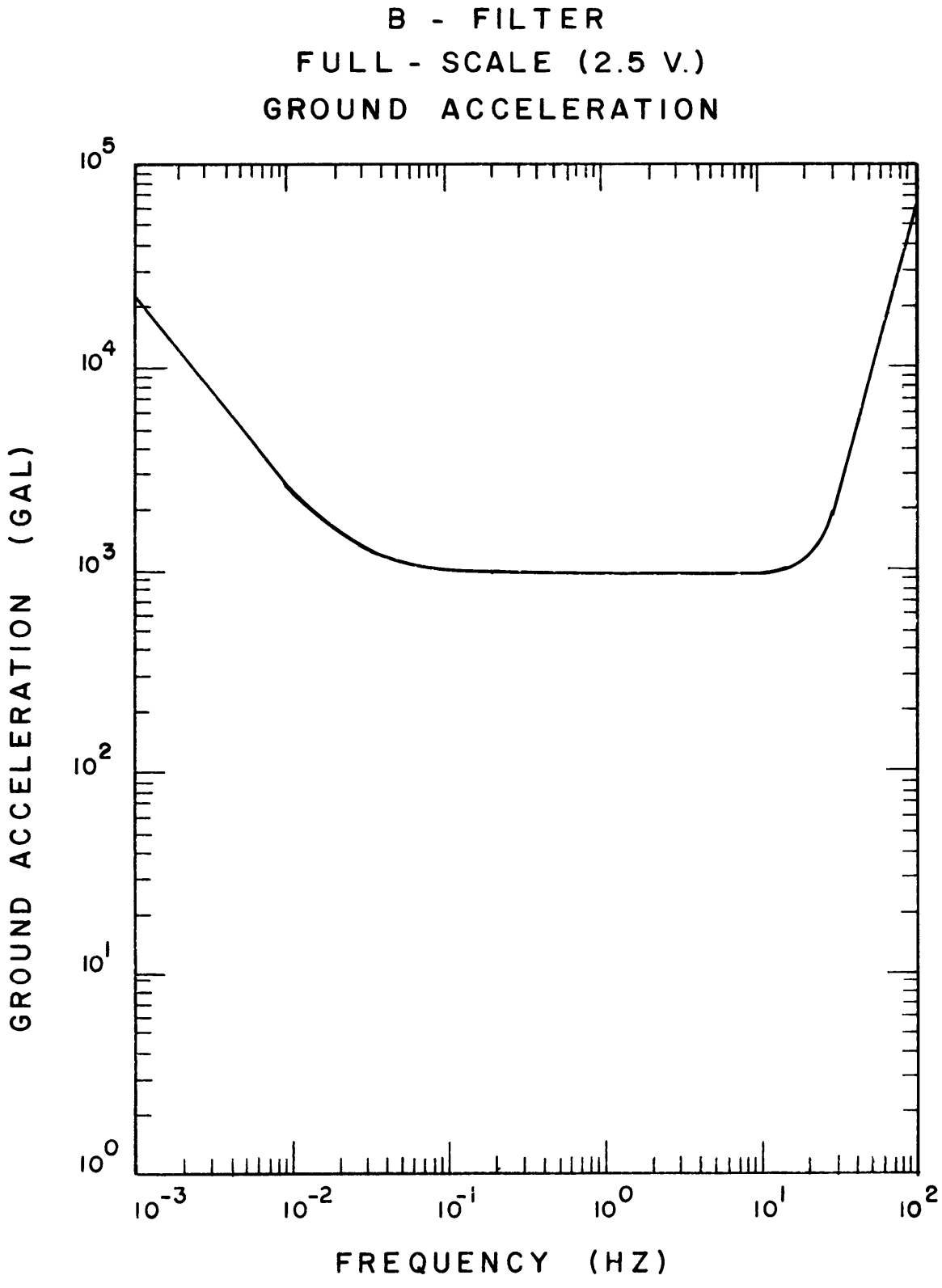
B - FILTER
FULL - SCALE (2.5 V.)
GROUND ACCELERATION
GROUND ACCELERATION (GAL)
10^5
10^4
10^3
10^2
10^1
10^0
10^{-3}
10^{-2}
10^{-1}
10^0
10^1
10^2
FREQUENCY (HZ)

Figure 12

A - FILTER SCHEMATIC DIAGRAM

6 May 1971

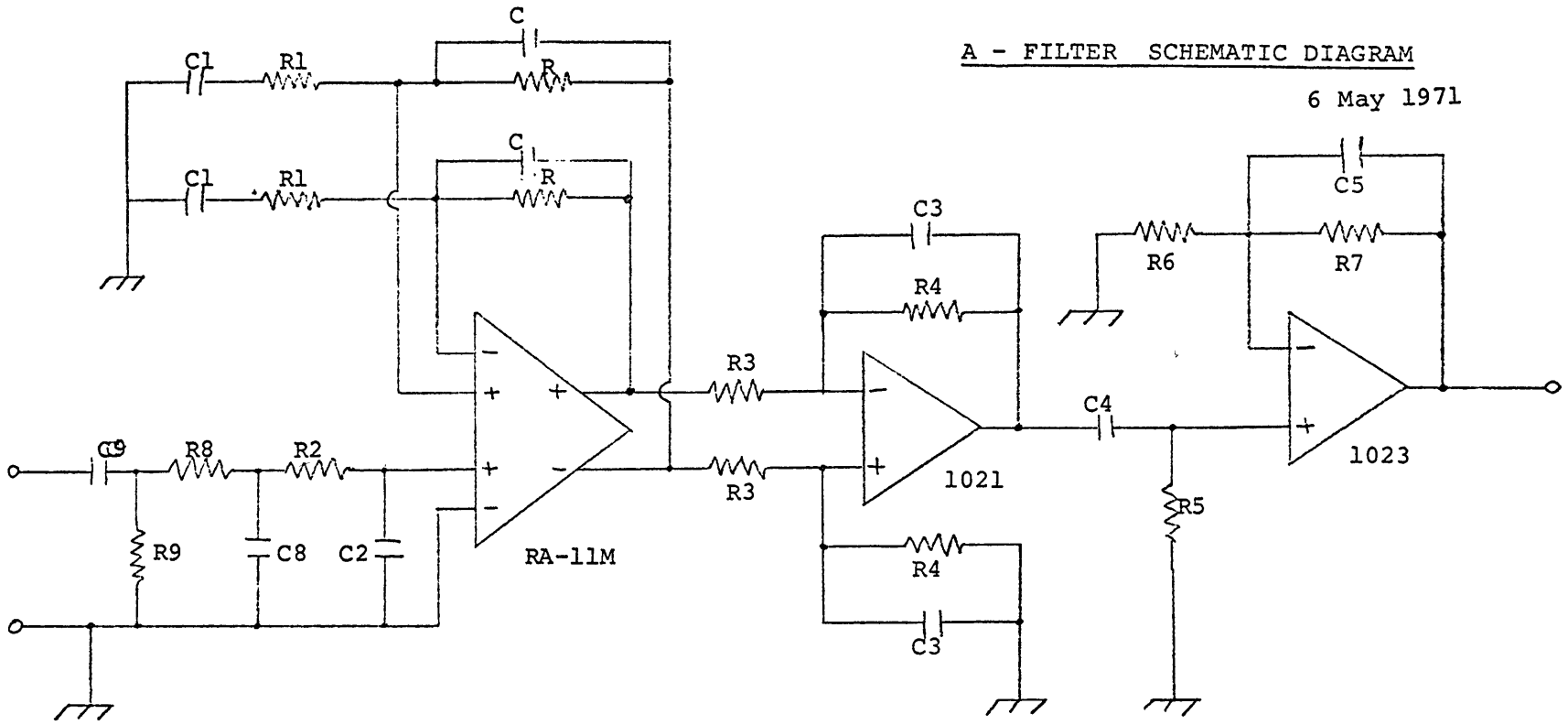

R	= 15.9 M	C	= 10 pf
R1	= 159 K	C1	= 100. μf
R2	= 15.9 M	C2	= 1.0 μf
R3	= 30 K	C3	= .015 μf
R4	= 1 M	C4	= 20. μf
R5	= 7.96 M	C5	= .15 μf
R6	= 100 K	C8	= 10. μf
R7	= 100 K	C9	= 5. μf
R8	= 1.59 M		
R9	= 5.6 M		

Figure 13

B - FILTER SCHEMATIC DIAGRAM

6 May 1971

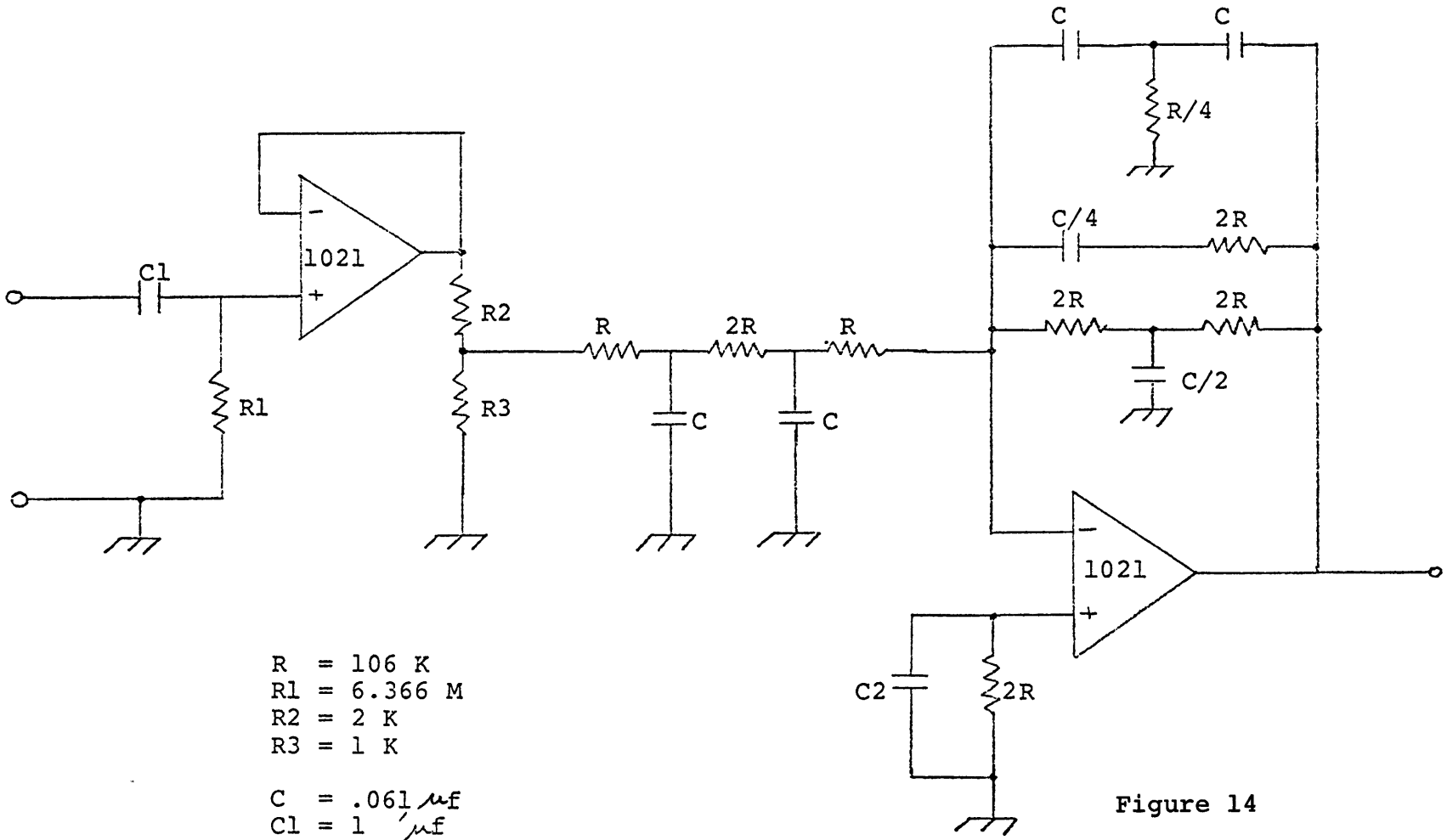

R = 106 K
R1 = 6.366 M
R2 = 2 K
R3 = 1 K

C = .061 μf
C1 = 1 μf
C2 = 160 pf

Figure 14

ARPA SEISMIC TELEMETRY SYSTEM POWER SUPPLIES

Figure 15

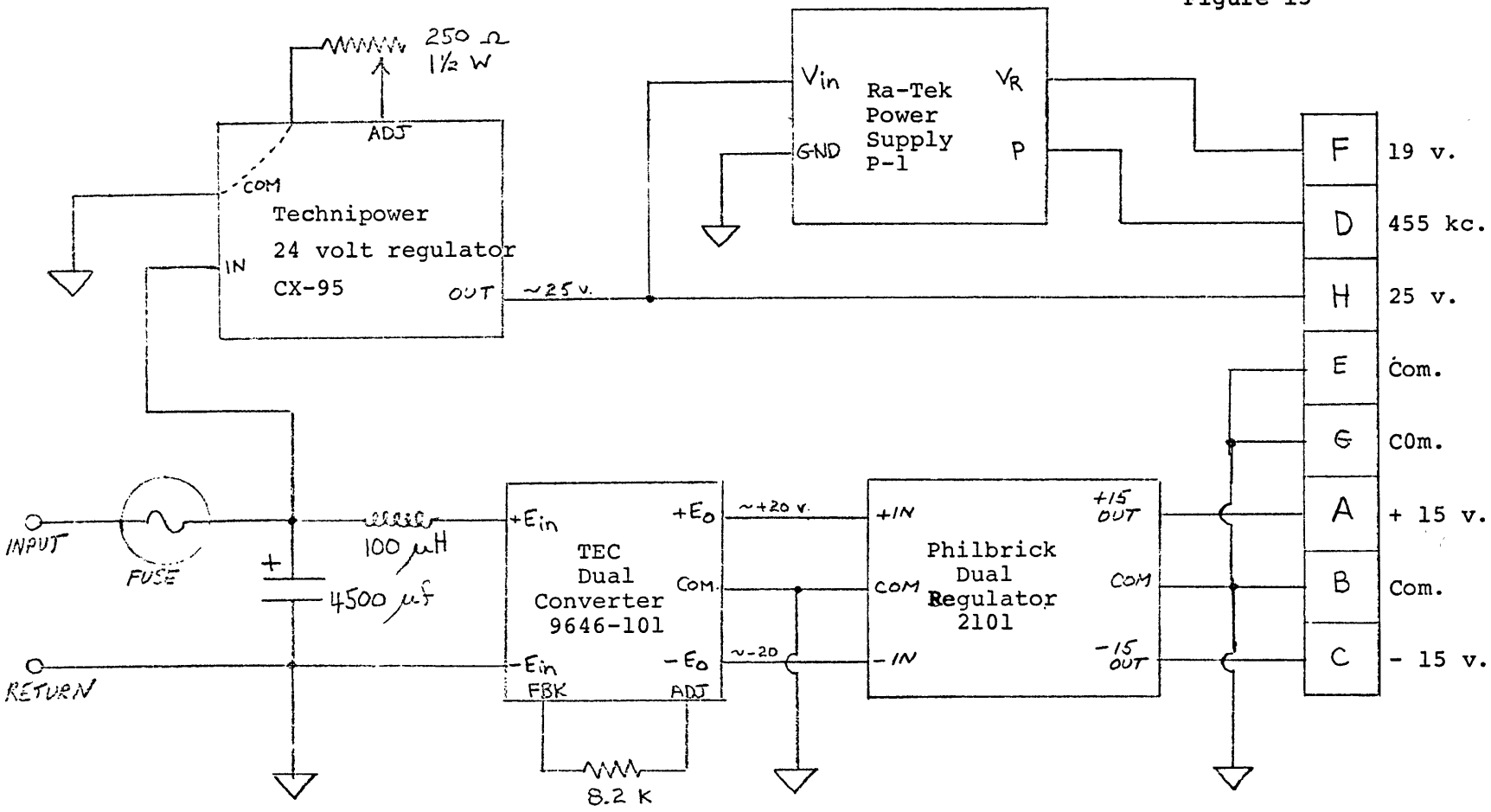

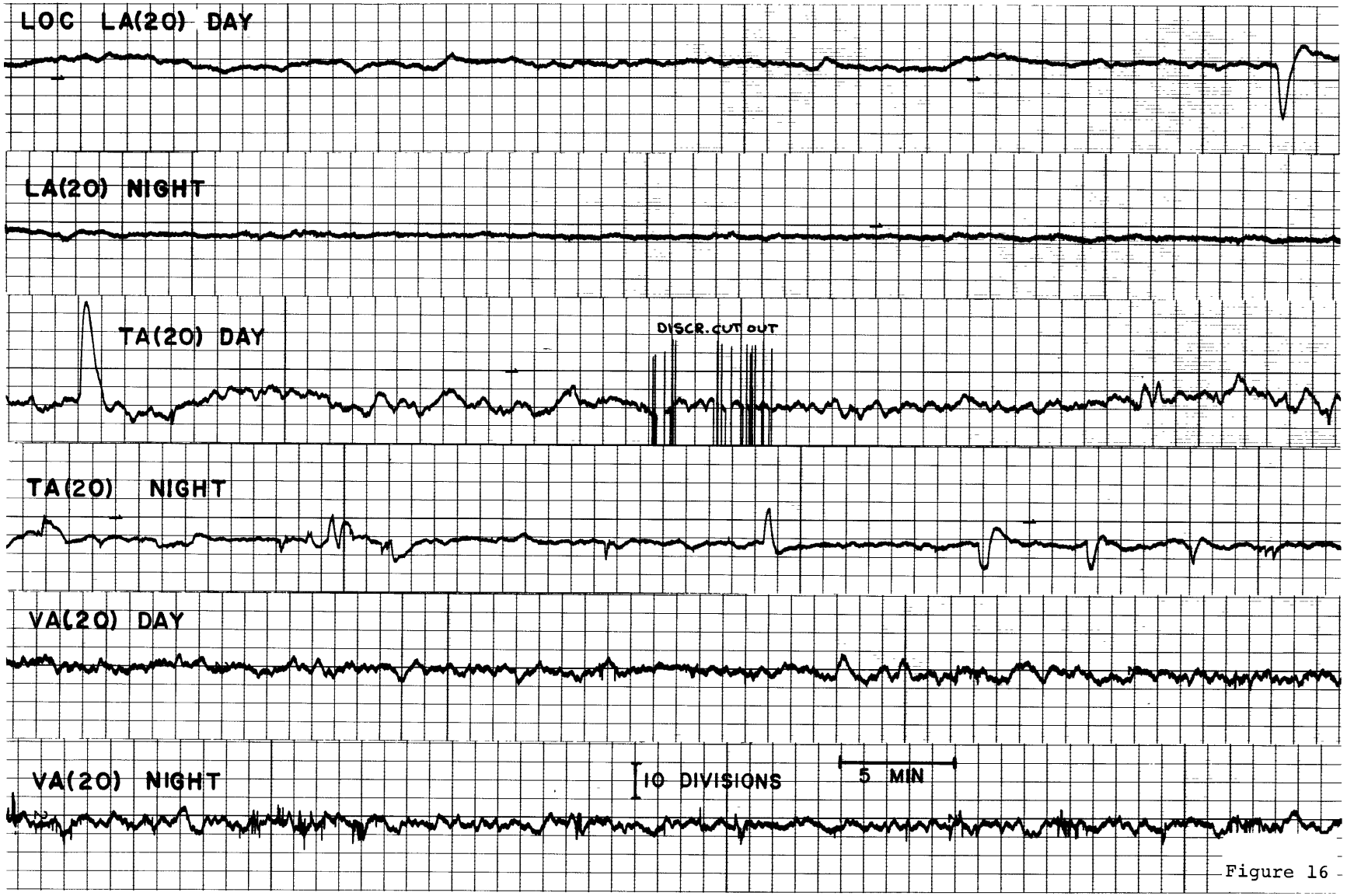
LOC LA(20) DAY
LA(20) NIGHT
TA(20) DAY
DISCR. CUT OUT
TA(20) NIGHT
VA(20) DAY
VA(20) NIGHT
10 DIVISIONS
5 MIN

Figure 16

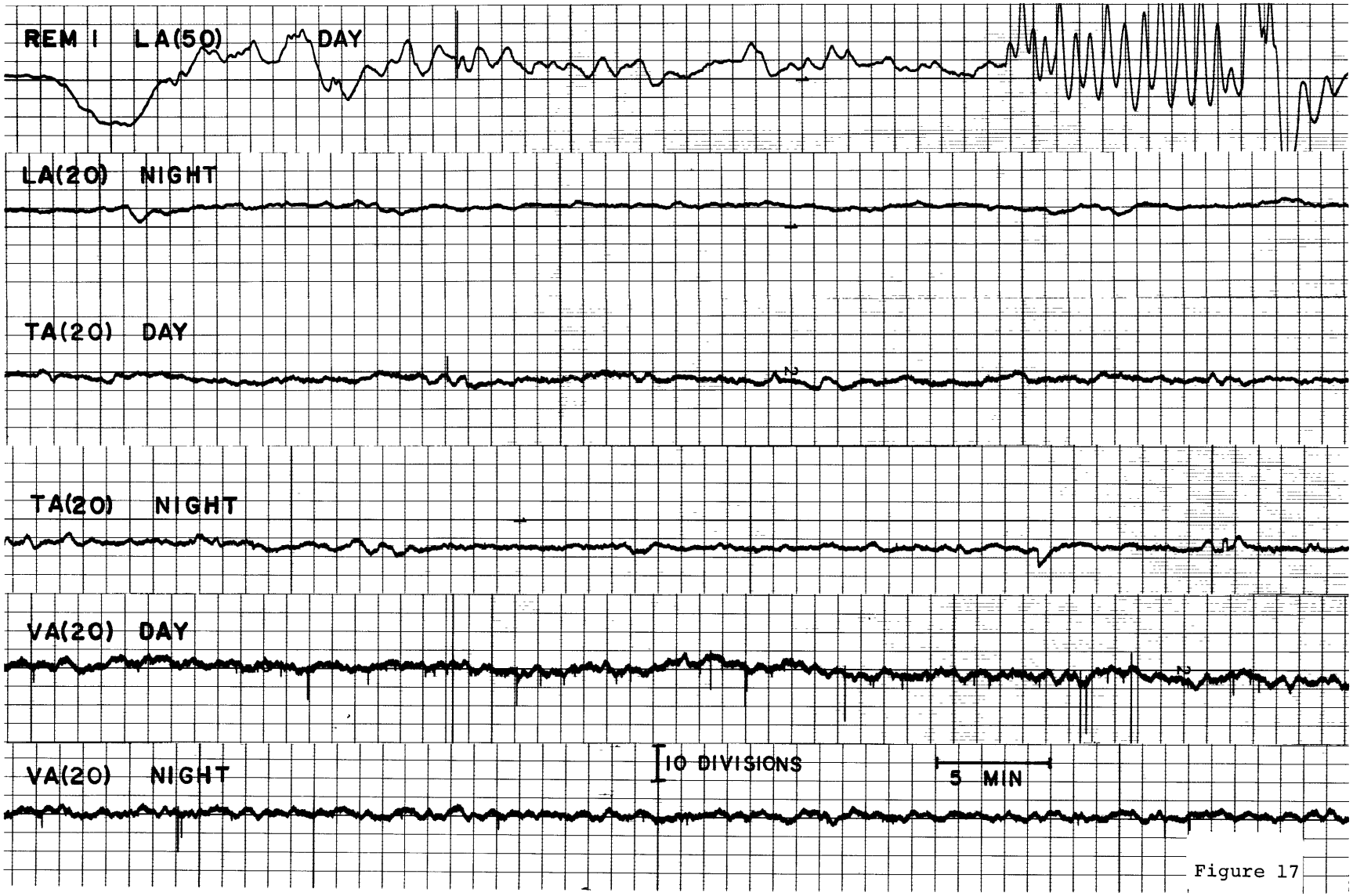
REM I LA(50) DAY
LA(20) NIGHT
TA(20) DAY
TA(20) NIGHT
VA(20) DAY
VA(20) NIGHT
10 DIVISIONS
5 MIN

Figure 17


REM 2 LA(50) DAY
LA(50) NIGHT
TA(20) DAY
TA(20) NIGHT
VA(50) DAY
VA(50) NIGHT
10 DIVISIONS
5 MIN

Figure 18

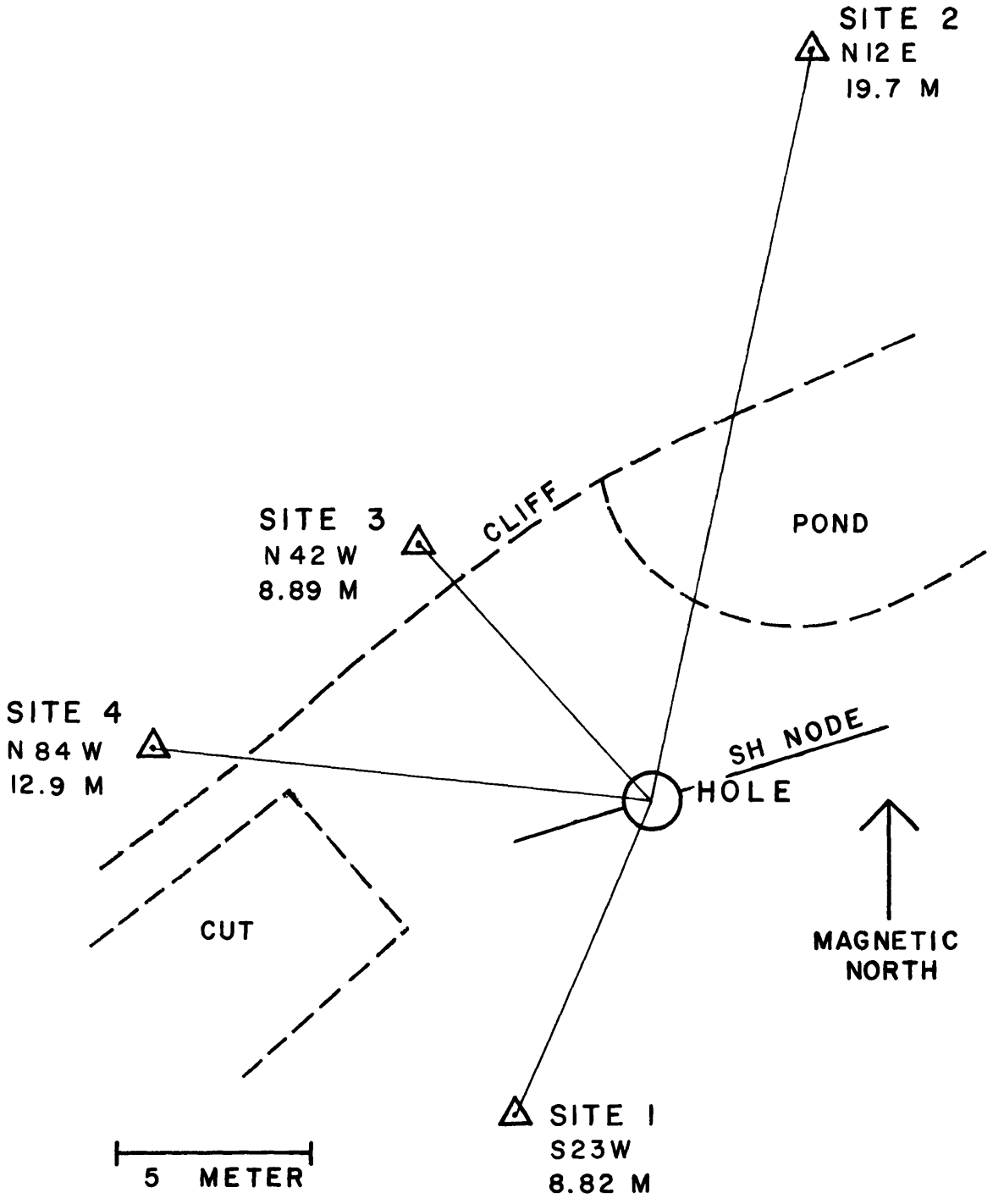

Figure 19

EXPERIMENT AREA

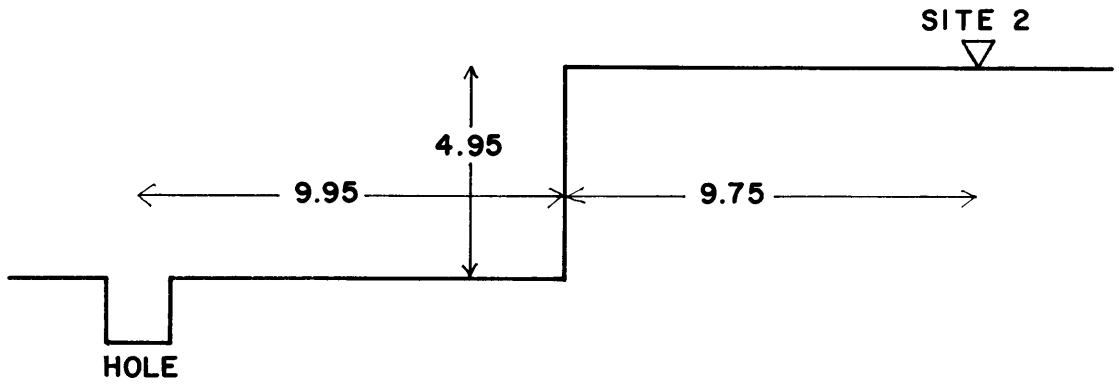
SITE 2
4.95
9.95
9.75
HOLE

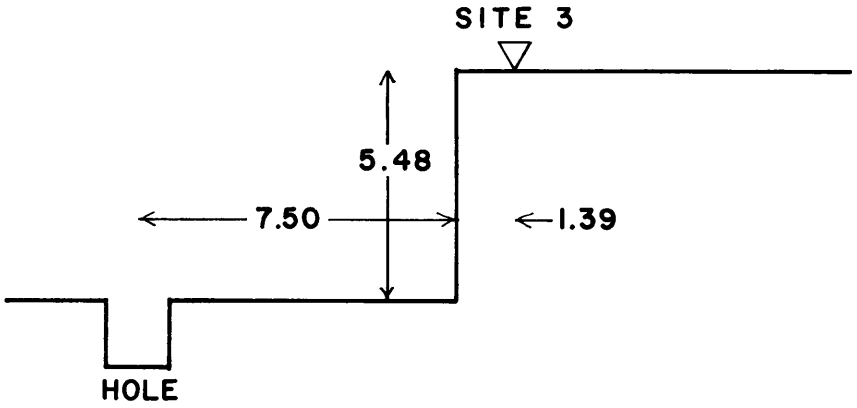
SITE 3
5.48
7.50
1.39
HOLE

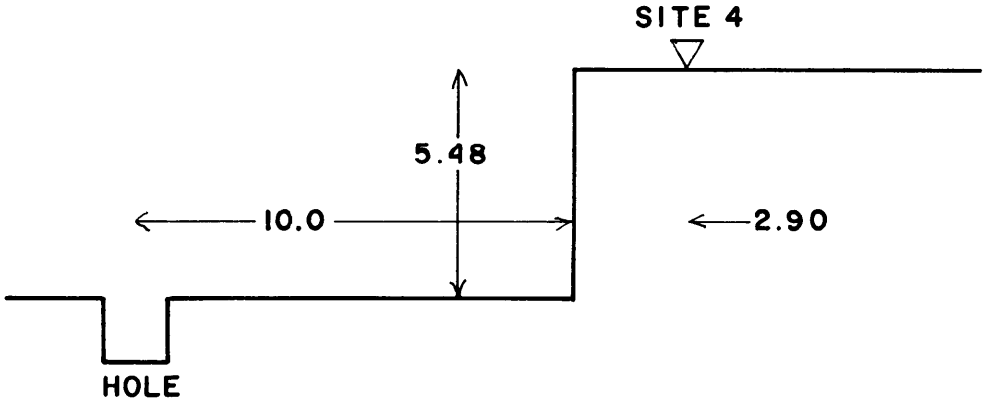
SITE 4
5.48
10.0
2.90
HOLE

Figure 20

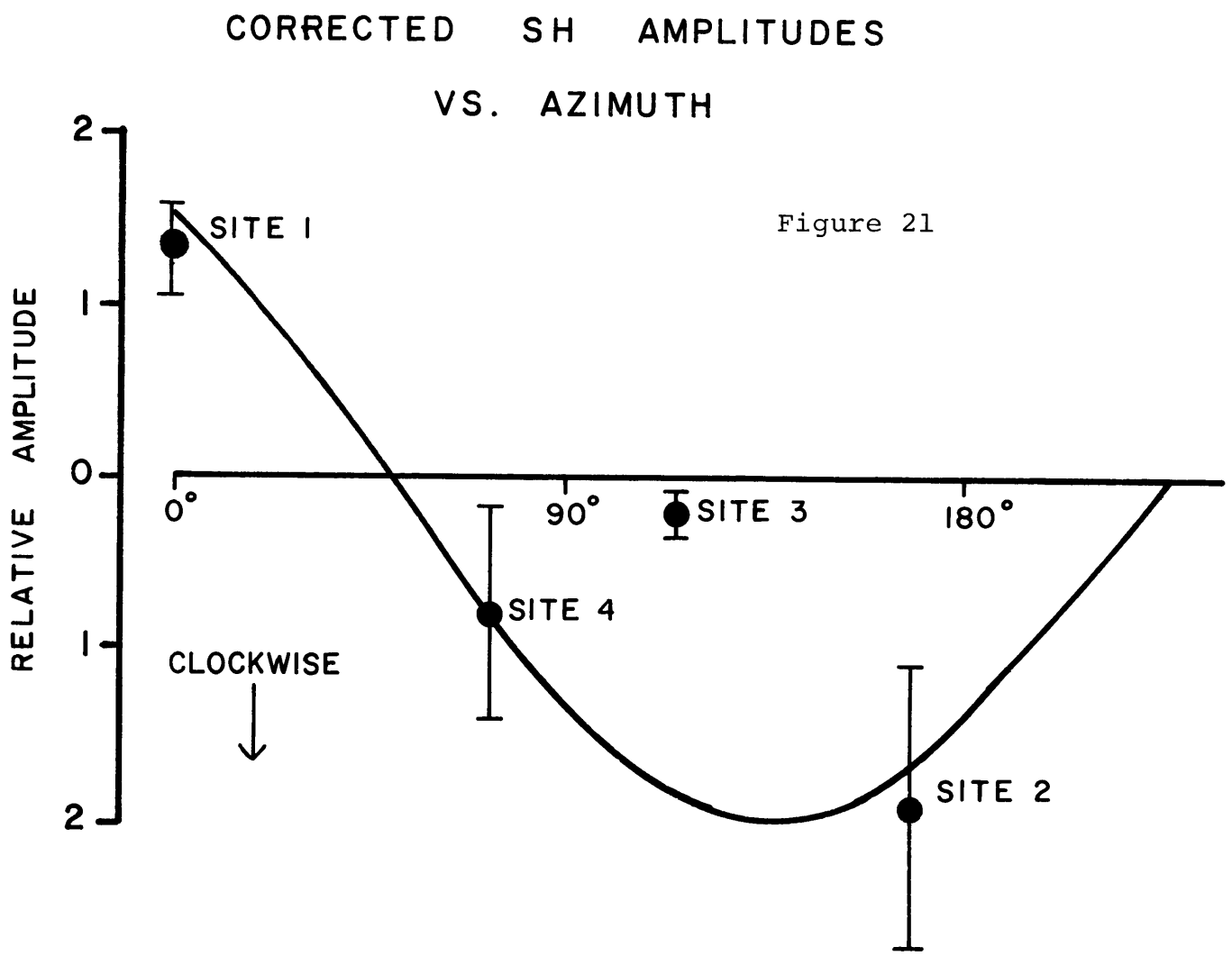
CORRECTED SH AMPLITUDES
VS. AZIMUTH
RELATIVE AMPLITUDE
2
1
0
1
2
SITE 1
0°
90°
SITE 3
180°
SITE 4
CLOCKWISE
SITE 2

Figure 21

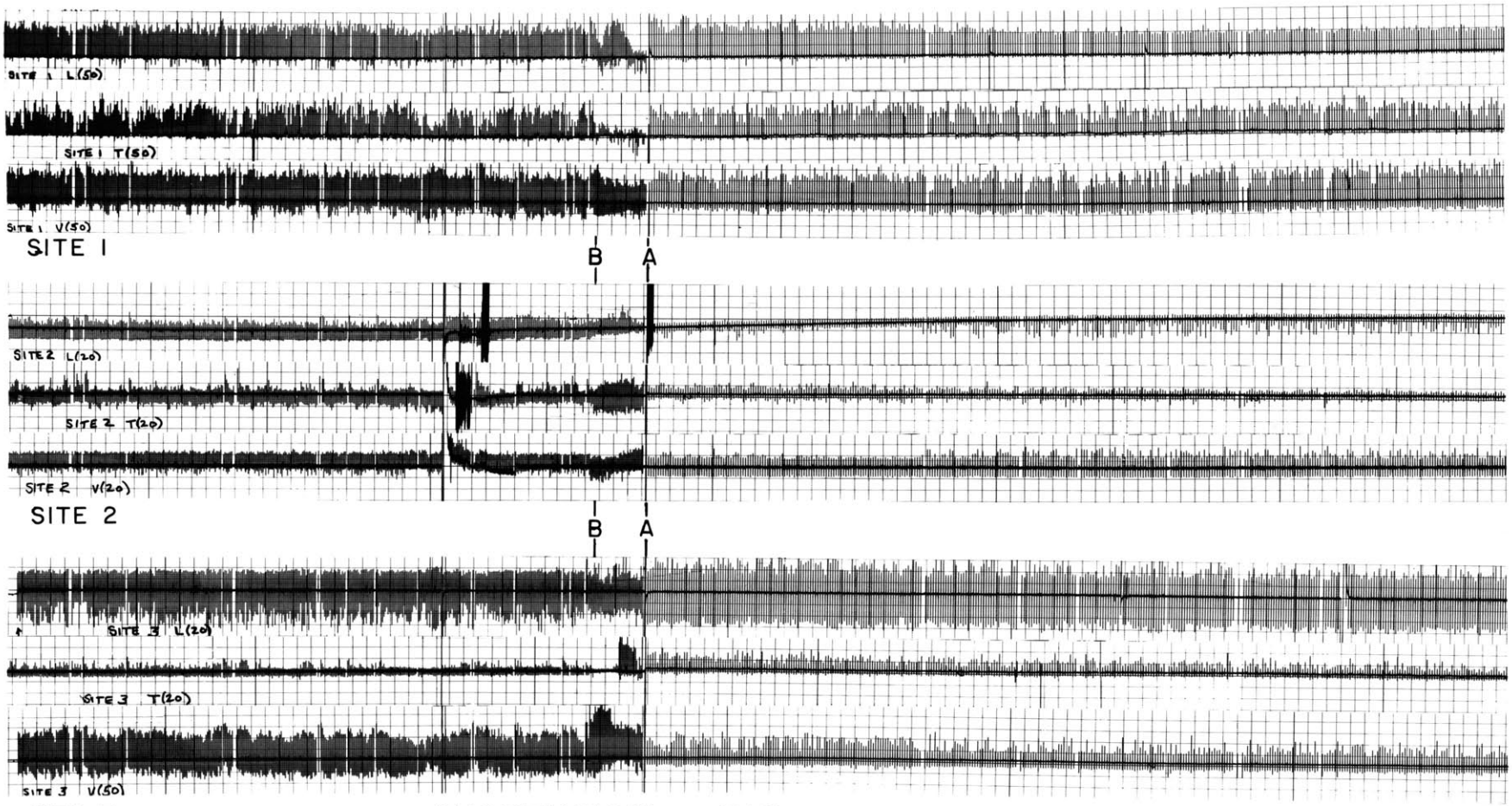
SITE 1 L(50)
SITE 1 T(50)
SITE 1 V(50)
SITE 1
B
A
SITE 2 L(20)
SITE 2 T(20)
SITE 2 V(20)
SITE 2
B
A
SITE 3 L(20)
SITE 3 T(20)
SITE 3 V(50)
SITE 3
SUSPENSION FAILURE
10 DIVISIONS
5 MIN

Figure 22